Supporting Information

Supporting Information for *In Situ* SERS and *In Situ* Raman: Interfacial Phenomena and Processes Deciphering

Jingyi Wei,[a‡] Sixian Yu,[b‡] Tianxiang Zhou,[a] Jing Shang,[a] Songling Liu,[c] Feng Han*,[a] Xiaodong Li*,[d] and Qi An*[a]

Supporting Information

To facilitate the reference of researchers, we have compiled an appendix on the Raman peaks and their corresponding behaviors under *in situ* systems. Within the in situ detection system, by correlating the Raman shift of the spectral peak to the ranges in our SI, researchers can identify vibrations relevant to their study system. Alternatively, if the species are known, researchers can search for the species name in the SI to obtain reference Raman shifts. However, it's important to note that the sequence of peak significance in the longitudinal order does not directly correlate with the transverse order found in the references. And this table should be used as a general guide rather than a definitive resource.

CONTENTS FOR SUPPORTING INFORMATION

[a] Engineering Research Center of Ministry of Education for Geological Carbon Storage and Low Carbon Utilization of Resources, Beijing Key Laboratory of Materials Utilization of Nonmetallic Minerals and Solid Wastes, National Laboratory of Mineral Materials, School of Material Sciences and Technology, China University of Geosciences, Beijing 100083, China. E-mail: hanfeng@cugb.edu.cn, an@cugb.edu.cn

[b] International Energy College, Jinan University, Guangdong 519070, China.

[c] School of Material Science and Engineering, Shanghai Jiao Tong University, Shanghai 200240, China.

[d] School of Chemical Engineering and Technology, Tianjin University, Tianjin 300072, China. E-mail: 18901029020@189.cn

‡ These authors contributed equally to this work.

50.0 cm^{-1}: [1]
1 Raman active vibrational bands of iodine species (begin)

60.0 cm^{-1}: [2]
1 Orthorhombic BiF_3 (o-BiF_3)

62.0 cm^{-1}: [2]
1 Metallic Bi

72.0 cm^{-1}: [3]
1 $NiTe_2$

76.0 cm^{-1}: [2]
1 o-BiF_3

88.0 cm^{-1}: [2]
1 Metallic Bi

99.0 cm^{-1}: [4]
1 E_2 (low) of ZnO_{100}

110.0 cm^{-1}: [1,5–7]
1 I_3^-
2 Raman active vibrational bands of I_3^- (begin)
3 The symmetric stretching mode of I_3^-
4 Vibration mode of I_3^-

115.0 cm^{-1}: [2]
1 o-BiF_3

120.0 cm^{-1}: [1]
1 Raman active vibrational bands of I_3^-(end)

123.0 cm^{-1}: [8]
1 AlSeCl

133.0 cm^{-1}: [8]
1 Al_2Se_3

135.0 cm^{-1}: [9,10]
1 $NiSe_2$
2 The interaction between S^{2-} and nickel

142.0 cm^{-1}: [8]
1 AlSeCl

143.0 cm^{-1}: [8]
1 E_1 mode of trigonal-phase Se

145.0 cm^{-1}: [11,12]
1 The E_g mode of anatase TiO_2

146.0 cm^{-1}: [13]
1 Surface Cu_2O (Cu_2O_{surf})

148.0 cm^{-1}: [10]
1 Elemental Sulfur (S_8)

149.0 cm^{-1}: [14]
1 S_8^{2-} peak of graphene/S

Continued on next page

150.0 cm^{-1}: [2,3,15–17]
1 cubic BiF_3 (c-BiF_3)
2 Bending or torsional vibrational modes of S-S bonds in elemental sulfur (S_8) (begin)
3 Roman peak of Li^2S_8
4 α-S_8
5 Vibration mode of S_8^{2-}

151.0 cm^{-1}: [18]
1 Symmetric bond stretching of S_8

152.0 cm^{-1}: [11]
1 The E_g mode of anatase TiO_2 (More defects)

155.0 cm^{-1}: [8,19,20]
1 Symmetric bond stretching mode of S_8^{2-}
2
3 TA (transverse acoustic) of graphite electrodes coated with Si layers of different thicknesses

156.0 cm^{-1}: [8]
1 Al_2Se_3

160.0 cm^{-1}: [5]
1 I_5^-

161.0 cm^{-1}: [21]
1 AlF_3 crystal
2 The interaction between S^{2-} and nickel

163.0 cm^{-1}: [6]
1 Symmetric stretching mode of I_5^-

165.0 cm^{-1}: [7]
1 Vibration mode of I_5^-

174.0 cm^{-1}: [22]
1 Reactive chloride ion species formed by electrochemical CER on Ru/RuO_2 electrode in Cl electrolyte

185.0 cm^{-1}: [8]
1 AlSeCl

187.0 cm^{-1}: [23]
1 A_g mode of monoclinic ZrO_2

192.0 cm^{-1}: [24]
1 F1 2g mode of spinel Co_3O_4

194.0 cm^{-1}: [10]
1 The vibration of Ni-S in rhombohedral Ni_3S_2

199.0 cm^{-1}: [16]
1 S_4^{2-}

200.0 cm^{-1}: [1,15,18,25,26]
1 Bending or torsional vibrational modes of S-S bonds in elemental sulfur (S_8) (end)
2 Vibration of Ni-S Bond in Ni_3S_2
3 Vibration mode of Li_2S_2
4 Raman active vibrational bands of I_3^-
5 F_{2g} modes of AO_4 units in AB_2O_4 spinel structure

Continued on next page

200.8 cm^{-1}:[16]
1 S_6^{2-}/S_4^{2-} Species

202.0 cm^{-1}:[14]
1 Bending mode of S_4^{2-}

206.0 cm^{-1}:[8]
1 Al_2Se_3

210.0 cm^{-1}:[27]
1 Solvated Mg-Cl cation species

212.0 cm^{-1}:[28]
1 A_g vibrational modes of Se-Se bonds in selenides

215.0 cm^{-1}:[16]
1 α-S_8

216.0 cm^{-1}:[10,29]
1 A_g mode of Se-Se stretching in Ru-$NiSe_2$
2 Vibration of Ni-S in rhombohedral Ni_3S_2

217.0 cm^{-1}:[25]
1 Vibration of Ni-S Bond in Ni_3S_2

218.0 cm^{-1}:[3,10,15]
2 Elemental sulfur (S_8)
3 Raman peaks of Li_2S_8

219.0 cm^{-1}:[14,17–19,30]
1 Bending of symmetric bonds in S_8
2 Cu_2O
3 Symmetric bond stretching mode of S_8^{2-}
4 S_8^{2-} peak of graphene/S
5 Vibration mode of S_8^{2-}

223.0 cm^{-1}:[15]
1 Hematite, Fe_2O_3

225.0 cm^{-1}:[8,12]
1 Solid electrolyte interface (SEI) layer of aluminum chlorochalcogenide
2 The E_g vibration mode of anatase TiO_2

235.0 cm^{-1}:[8]
1 A_1 mode of trigonal-phase Se

236.6 cm^{-1}:[31]
1 The E_g phonon mode of Ni

240.0 cm^{-1}:[28]
1 T_g vibrational modes of Se-Se bonds in selenides

242.0 cm^{-1}:[25]
1 Fe-O bond of α-FeOOH

243.0 cm^{-1}:[32,33]
1 NO_2 species
2 Longitudinal mode of surface oxygen
3 S-Ag stretching vibration between H_2SO_4 component and Ag

Continued on next page

249.0 cm^{-1}:[34]
1 Lepidocrocite (γ-FeOOH)

250.0 cm^{-1}:[9,21,35]
1 $NiSe_2$
2 The characteristic peak of $Co(OH)_2$
3 Al-F bonds in $Na_5Al_3F_{14}$ crystal (νs)
4 Terminal SS bond (begin)

251.0 cm^{-1}:[36]
1 The second-order effect (SOE) of anatase TiO_2

256.0 cm^{-1}:[8]
1 Amorphous Se

258.0 cm^{-1}:[37]
1 Second order transverse acoustic mode of CeO_2 lattice (2TA)

259.0 cm^{-1}:[38]
1 Bending vibration of O-W-O

260.0 cm^{-1}:[39]
1 E_g mode for $Co(OH)_2$

262.0 cm^{-1}:[40]
1 The second-order transverse acoustic mode of FCC fluorite phase of CeO_2

268.0 cm^{-1}:[41]
1 The E_g mode of Co-O bonds

269.0 cm^{-1}:[23]
1 The E_g mode of Co-O bonds

273.0 cm^{-1}:[42]
1 CuO

281.0 cm^{-1}:[43]
1 A_g translation mode
2 Symmetric stretching mode of FeS (begin)

282.0 cm^{-1}:[15]
1 Amorphous Mackinawite/Mackinawite

285.0 cm^{-1}:[44]
1 A_g mode of CuO

288.94 cm^{-1}:[45]
1 The E_g mode of metal sulfur bonds in $Co(Zn)S_2$/CC

289.0 cm^{-1}:[15,46]
1 CuO
2 Hematite

290.0 cm^{-1}:[47]
1 E-type vibrations of h-$Co_{0.34}Fe_{0.33}Ni_{0.33}$-LDH

292.0 cm^{-1}:[48]
1 Frustrated rotation of Cu-CO

296.0 cm^{-1}:[13,49]
1
2 Crystalline CuO nanoparticles

Continued on next page

298.0 cm^{-1}: [15,16,44]
1 Ferrites
2 S_6^{2-}
3 S_4^{2-}
4 Restricted rotation of adsorbed CO
5 Symmetric stretching mode of FeS (end)

300.0 cm^{-1}: [10,17]
1 Vibration of Ni-S in rhombohedral Ni_3S_2
2 The vibration mode of mid-length LiPS

303.0 cm^{-1}: [13,30]
1 CuC stretching and rotation mode of adsorbed CO (end)

304.0 cm^{-1}: [25]
1 Vibration of Ni-S Bond

305.0 cm^{-1}: [23]
1 δInO_6 structural units (δInO_6)

306.0 cm^{-1}: [38]
1 $\delta(W[=O]_2)$ of crystalline Na_2WO_4 phase

310.0 cm^{-1}: [20,50]
1 Adsorbed phosphate ions
2 LA (longitudinal acoustics) of graphite electrodes coated with Si layers of different thicknesses

312.66 cm^{-1}: [51]
1 A_{1g} peak of SnS_2

319.0 cm^{-1}: [38]
1 Bending vibration of O-W-O

320.0 cm^{-1}: [50]
1 Adsorbed phosphate ions

321.0 cm^{-1}: [21,22,52]
1 Reactive chloride ion species formed by electrochemical CER on Ru/RuO_2 electrode in Cl^- electrolyte
2 Ni-LDH
3 Symmetric stretching vibration B_{2g} mode of Al-F bonds in $Na_5Al_3F_{14}$ crystal (ν_s)

324.0 cm^{-1}: [19,53]
1 Asymmetric deformation modes of VO_4^{3-}
2 Li_2S_6

325.0 cm^{-1}: [10]
1 The interaction between S^{2-} and nickel

326.0 cm^{-1}: [18]
1 Vibration mode of Li_2S_6

330.0 cm^{-1}: [4]
1 E_2 (High) - E_2 (low) of ZnO_{100}

331.0 cm^{-1}: [30]
1 CuO

334.0 cm^{-1}: [23]
1 Monoclinic ZrO_2

Continued on next page

336.0 cm^{-1}: [43]
1 E_{2g} mode of $La(OH)_3$

339.0 cm^{-1}: [21]
1 B_g mode of Al-F bonds in Na_3AlF_6 (Calculation)

342.0 cm^{-1}: [10]
1 Vibrations of Ni-S in rhombohedral Ni_3S_2

343.0 cm^{-1}: [42]
1 Ni oxide NiO

345.0 cm^{-1}: [23]
1 Stretching vibrations of the InOIn structures

346.0 cm^{-1}: [22]
1 Reactive chloride ion species formed by electrochemical CER on Ru/RuO_2 electrode in Cl^- electrolyte

351.0 cm^{-1}: [25,54]
1 Vibration of Ni-S Bond in Ni_3S_2
2 Mn-OH is deuterated to Mn-OD

352.0 cm^{-1}: [44]
1 Restricted rotation of Cu-CO stretching

355.0 cm^{-1}: [13]
1 CuC stretching and rotation mode of adsorbed CO

359.0 cm^{-1}: [21]
1 Symmetric stretching vibration E_g mode of Al-F bonds in $Na_5Al_3F_{14}$ crystal (υs)

360.0 cm^{-1}: [54]
1 MnOH is deuterated to MnOD

360.51 cm^{-1}: [51]
1 A_g^1 peak of black phosphorus (BP)

361.0 cm^{-1}: [21]
1 Ag mode of Al-F bonds in Na_3AlF_6 (Calculation)

363.0 cm^{-1}: [35]
1 The characteristic peaks of CoOOH

365.0 cm^{-1}: [55]
1 Cu-CO stretching vibration

367.0 cm^{-1}: [48]
1 Stretch of Cu-CO

374.0 cm^{-1}: [56,57]
1 Peak of $MoO_{3-x}(0<x<1)$
2 Formation of $Na_2O(UO_3 \cdot H_2O)$ x precipitation

375.0 cm^{-1}: [58]
1 Active CoOOH intermediate species

376.0 cm^{-1}: [59]
1 Terminal Mn-O (H) tunnel or surface expansion

378.0 cm^{-1}: [34]
1 Lepidocrocite (γ-FeOOH)

Continued on next page

380.0 cm^{-1}: [23]
1 Monoclinic ZrO_2

383.0 cm^{-1}: [60]
1 $SrTiO_3$ unit cell via La and Co doping (STLC)

384.0 cm^{-1}: [49]
1 Anatase vibration of TiO_2

386.0 cm^{-1}: [21,25]
1 Fe-O bond of α-FeOOH
2 AlF_3 crystal

390.0 cm^{-1}: [45]
1 A_g mode of metal-S in $Co(Zn)S_2$/CC

398.0 cm^{-1}: [3,14]
1 Long chain LiPSs (Li_2S_6)
2 Characteristic Raman peaks of long-chain Li_2S_6

399.0 cm^{-1}: [12,61]
1 Ag-O vibration
2 B_{1g} vibration mode of anatase TiO_2

399.5 cm^{-1}: [16]
1 S_6^{2-}/S_4^{2-} Species

400.0 cm^{-1}: [15,17,20,62,63]
1 corundum
2 H_2SO_4 electrolyte
3 LO (longitudinal optics) of graphite electrodes coated with Si layers of different thicknesses
4 Vibration mode of short chain LiPS
5 Bending vibration of C-S bonds
6 Stretching vibration of S_8 (begin)

401.9 cm^{-1}: [18]
1 Vibration mode of Li_2S_6

404.0 cm^{-1}: [15]
1 Hematite

405.0 cm^{-1}: [64]
1 Vibration of Au-O bonds

409.0 cm^{-1}: [65]
1 NiO

410.0 cm^{-1}: [66]
1 Characteristic Raman peaks of α-FeOOH phase

412.0 cm^{-1}: [13]
1 Cu_2O (Cu_2O_{surf})

415.0 cm^{-1}: [20,67,68]
1 The vibration mode of Cu_2O
2 S_n^{2-}
3 Raman peaks of amorphous silicon (a-Si)

416.0 cm^{-1}: [19,21]
2 Li_2S_4

418.0 cm^{-1}: [69]
1 Lattice vibrations of Mo-O bonds

Continued on next page

420.0 cm^{-1}: [58,70–72]
1 Bending of symmetric oxygen cages
2 F_{2g} symmetric vibration of CeO_2
3 Metal adsorbate stretching vibration of linear CO bonds (AuNi COL)
4 Network bending mode of SiO_2

422.0 cm^{-1}: [36]
1 The E_g vibration mode of anatase TiO_2

426.0 cm^{-1}: [73]
1 The vibration mode of Co-O

431.39 cm^{-1}: [51]
1 B_{2g} peak of BP

432.0 cm^{-1}: [74]
1 The vibration mode of RuO_2

437.0 cm^{-1}: [75]
1 E_2 high mode of ZnO

439.0 cm^{-1}: [4]
1 E_2 (High) of ZnO_{100}

440.0 cm^{-1}: [61]
1 Bulk oxygen

441.0 cm^{-1}: [76]
1 Au-Bi_2O_3-3

443.0 cm^{-1}: [68]
1 S_n^{2-}
2 $S_2O_3^{2-}$

445.0 cm^{-1}: [14,76–78]
1 Au-Bi_2O_3-3
2 β-$Ni(OH)_2$
3 $Na_3Al_3CF_8$
4 Bending mode of S_4^{2-}

446.0 cm^{-1}: [12,18,79]
1 The E_g bending vibration mode of MO bonds in MOH species
2 Vibration mode of Li_2S_4
3 B_g vibration mode of anatase TiO_2

450.0 cm^{-1}: [47,76,80–83]
1 h-$Co_{0.34}Fe_{0.33}Ni_{0.33}$-LDH
2 Ni (II) - OH
3 Bi_2O_3
4 Bonding between Mo atom and top S atom (v (Mo_3-S))
5 CoII-OH vibration of $Co(OH)_2$
6 MII-OH of Co and Fe
7 ClO_4^- ions in polycarbonate solution

451.0 cm^{-1}: [35,76,84]
1 The Ni-O vibration peak of NiFeLDH
2 Bi_2O_3
3 Asymmetric breathing mode of oxygen atoms surrounding cerium ions in CeO_2

452.0 cm^{-1}: [18,25,85]
1 F_{2g} symmetric vibration (Ce-O-Ce stretching)
2 Ni-O bond stretching vibration
3 Vibration mode of Li_2S_2

Continued on next page

453.0 cm^{-1}: [52,85]
1 Ce-O bond
2 Ni-LDH

455.9 cm^{-1}: [16]
1 S_6^{2-}/S_{42-} Species

456.0 cm^{-1}: [79]
1 The stretching vibration of M-O bonds

457.0 cm^{-1}: [86,87]
1 NiFe-LDH@NF Ni-O vibration in $Ni(OH)_2$ phase on the surface
2 Bending and stretching vibration of Ni-O in NiOOH

457.97 cm^{-1}: [51]
1 A_g^2 peak of BP

458.0 cm^{-1}: [85]
1 Symmetric tensile vibration of Ce-O

460.0 cm^{-1}: [41,77,88–91]
1 E_g-CO^{2+}-OH
2 Triple Degeneracy Mode of F_{2g} Mode in CeO_2
3 O-Co-O bending mode
4 O-Co-O
5 α-$Ni(OH)_2$
6 Perchlorate electrolyte
7 The E_g vibrational modes of Co-O species

460.9 cm^{-1}: [92]
1 CoO_2

461.0 cm^{-1}: [3]
1 Long chain LiPSs (Li_2S_5+Li_2S_4)

462.0 cm^{-1}: [37]
1 Vibration model of octahedral local symmetry from the CeO_2 lattice (F_{2g})

463.0 cm^{-1}: [35,93]
1 The characteristic peaks of CoOOH
2 Ni-O vibration of defective NiCoLDH nanocrystals

464.0 cm^{-1}: [49]
1 Vibration of CeO_2 nanoparticles

465.0 cm^{-1}: [40,80]
1 Ni-O bond
2 The first-order F_{2g} symmetric vibration of CeO_2

465.5 cm^{-1}: [31]
1 A_g phonon modes of Ni

467.0 cm^{-1}: [94]
1 The peak of β-$Ni(OH)_2$ phase

467.6 cm^{-1}: [46]
1 Cu_2O

468.0 cm^{-1}: [95]
1 Ni-O vibration in γ-NiOOH

Continued on next page

469.0 cm^{-1}: [28,93]
1 High valence nickel iron hydroxide (NiFe)OOH
2 Characteristic peaks of NiCoOOH

470.0 cm^{-1}: [19,20]
1 Li_2S_6/Li_2S_4 mixture
2 Vibration modes of TO (transverse optic) in graphite electrodes coated with Si layers of different thicknesses

472.0 cm^{-1}: [3,10,96]
1 Elemental sulfur (S_8)
2 The E_g band of $LiNiO_2$(LNO)
3 Raman peaks of Li_2S_8

473.0 cm^{-1}: [25,62,80,84,97]
1 C-C_{ring} vibration of 4-AP and 4-NP(4-nitrophenol)
2 Active NiOOH species (γ-NiOOH)
3 Metal (M) O Vibration in Metal OOH
4 γ-NiOOH
5 E_g Ni-O bending vibration mode in NiOOH

474.0 cm^{-1}: [18,29,98]
1 NiOOH
2 F_{2g} vibration mode of $NiCo_2O_4$
3 Anti-symmetric bond bending of S_8

475.0 cm^{-1}: [9,10,16,25,43,70]
1 Depolarized E_g mode of γ-NiOOH phase (bending vibration of oxygen atoms on a plane) of γ-NiOOH phase
2 NiOOH
3 Ni-O vibration in NiOOH
4 The E_g, Ni-O bending vibration modes of γ-NiOOH
5 (Co/Fe) O (OH) structure

476.0 cm^{-1}: [35,86,99]
1 Ni-OOH vibration
2 Ni-O vibration of NiOOH
3 The characteristic peak of CoO_2

477.0 cm^{-1}: [14,89,100]
1 Ni-O bending vibration of γ-NiOOH phase
2 The E_g band of NiOOH
3 S_8^{2-} peak of graphene/S

478.0 cm^{-1}: [17,19,101]
1 The E_g bending mode of γ-NiOOH
2 Symmetric bond stretching mode of S_8^{2-}
3 Vibration mode of S_8^{2-}

479.0 cm^{-1}: [65]
1 E_g bending vibration in NiOOH

480.0 cm^{-1}: [35,63,66,88,91,102–104]
1 Formation of CoOOH
2 E_g Ni^{2+}-O bending
3 Ni(III)-O bending (δ) in NiOOH
4 Polarized A_{1g} mode (stretching) of Ni^{III}-O in NiOOH
5 Characteristic Raman peaks of γ-NiOOH phase
6 The characteristic peak of CoO_2
7 The stretching vibration of S-S bonds
8 The E_g vibrational modes of Co-O species

Continued on next page

481.0 cm^{-1}:[18]
1 Depolarization of γ-NiOOH in E_g mode (Bending)

482.0 cm^{-1}:[105]
1 Typical bending δ(NiIII-O)

483.0 cm^{-1}:[87]
1 Vibration of Co(OH) x

485.0 cm^{-1}:[24,30,96]
1 $Co(OH)_2$-phase
2 The E_g mode of spinel Co_3O_4
3 The E_g band of LNO
4 NiOOH species

487.0 cm^{-1}:[30,106]
1 Bending of Ni^{3+}-O
2 NiOOH species
3 Tri- and tetra-cycloxiloxane rings of SiO_2

488.0 cm^{-1}:[58,72]
1 F_{2g} symmetric vibration mode of CeO_2
2 D1 and D2 defect modes of tri- and tetra-cyclotrisiloxane in SiO_2

489.0 cm^{-1}:[35,57]
1 The characteristic peaks of CoOOH
2 Adsorbed uranyl

494.0 cm^{-1}:[107]
1 Characteristic of vibrational modes directly involving Fe species in MOFs catalyst

494.84 cm^{-1}:[45]
1 The stretching vibration of Co-O bonds

495.0 cm^{-1}:[45,100]
1 Disordered Ni-OH
2 Co(Zn)OOH

497.0 cm^{-1}:[108]
1 V-O-Ag bonds with different coordination structures in $Ag_{1.2}V_3O_8$

497.8 cm^{-1}:[92]
1 CoOOH species

498.0 cm^{-1}:[30]
1 $Cu(OH)_2$

500.0 cm^{-1}:[22,24,54,78,80,83,91,109,110]
1 CoOOH
2 Terminal SS bond (end)
3 Defective NiOOH or $Ni(OH)_2$
4 Interplanar vibration of adjacent MnO_2 nanosheets
5 The E_g mode of nanocrystalline RuO_2
6 The bending mode of Co-O-Co
7 Raman spectra of molten NaF-AlF_3-Al_4C_3 salts
8 Uncoordinated Si atoms near the surface of poly-c Si thin films
9 The E_g vibrational modes of Co-OOH species

501.0 cm^{-1}:[35]
1 The characteristic peaks of CoOOH

Continued on next page

502.0 cm^{-1}:[23]
1 $\nu(InO_6)$ of InO_6 structural units

506.0 cm^{-1}:[35]
1 The characteristic peak of $Co(OH)_2$

507.0 cm^{-1}:[59]
1 Out of plane symmetric stretching vibration of Mn-O in MnO_6

507.7 cm^{-1}:[18]
1 Vibration mode of Li_2S_3

509.0 cm^{-1}:[14,42,58]
1 Active CoOOH intermediate species
2 NiO
3 Characteristic Raman peaks of long-chain Li_2S_6

510.0 cm^{-1}:[81]
1 Terminal $[S_2]^{2-}$ ($\nu(S\text{-}S)_{te}$)

512.0 cm^{-1}:[12,49]
1 The vibration mode of anatase
2 A_{1g} vibration mode of anatase TiO_2

515.0 cm^{-1}:[35,44]
1 Characteristic peaks of Co_3O_4
2 OH group

517.0 cm^{-1}:[30]
1 The vibration of $Ni(OH)_2$

518.0 cm^{-1}:[65,74,77]
1 Fe-free and the Fe-containing electrolyte
2 β-$Ni(OH)_2$
3 Ru-O characteristic peaks belonging to RuO_2

519.0 cm^{-1}:[79]
1 A_{1g} stretching vibration mode of M-O bonds in MOH species

520.0 cm^{-1}:[20,83]
1 Crystalline peak of Si
2 Bulk c-Si

521.0 cm^{-1}:[93,111]
1 Ni-O vibrations of defective or disordered NiCo LDH nanocrystals
2 Li Si alloy

522.0 cm^{-1}:[87]
1 Co-O vibration in NCMO

523.0 cm^{-1}:[35,112]
1 The characteristic peak of $Co(OH)_2$
2 Nafion molecule

524.0 cm^{-1}:[35]
1 The characteristic peak of $Co(OH)_2$

525.0 cm^{-1}:[13,24,31,34,67]
1 $CuO_x/(OH)_y$ species
2 Lepidocrocite (γ-FeOOH)
3 The characteristic peaks of M(metal)-OOH
4 F2 2g mode of spinel Co_3O_4
5 The vibration mode of Cu_2O (begin)

Continued on next page

526.0 cm^{-1}: [41,47,55,88,100,101,113]

1 The vibration mode of Cu_2O
2 Adsorption of primary intermediates (such as $CO_{2\,ad}$) on Cu
3 M-O vibration of h-$Co_{0.34}Fe_{0.33}Ni_{0.33}$-LDH
4 A_{1g} Ni^{2+}-O stretching
5 Formation of FeOOH intermediates
6 Co-O symmetric stretching mode of $Co(OH)_2$
7 Co-O
8 FeOOH

527.0 cm^{-1}: [93]

1 Characteristic peaks of NiCoOOH

528.0 cm^{-1}: [13,65,95]

1 Surface Cu_2O (Cu_2O_{surf})
2 Thin, disordered NiFe-LDH
3 α-$Ni(OH)_2$

530.0 cm^{-1}: [26,66,80,91]

1 Defective NiOOH or $Ni(OH)_2$
2 Ni(II)-O
3 Typical Raman features of Ni-Fe-LDH
4 T_{2g} mode of CoO/rGO
5 A_g vibrational modes of CoOOH species (begin)

531.0 cm^{-1}: [25]

1 Ni-O stretching vibration

532.0 cm^{-1}: [21]

1 A_g mode of Al-F bond in Na_3AlF_6 (Calculation)

534.0 cm^{-1}: [67]

1 The vibration mode of Cu_2O (end)

536.0 cm^{-1}: [21]

1 A_{1g} mode of Al-F bonds in $Na_5Al_3F_{14}$ crystal(ν_s)

538.0 cm^{-1}: [86]

1 Ni-O vibrations in surface $Ni(OH)_2$ phase of NiFe-LDH@NF

541.0 cm^{-1}: [84]

1 The Ni-O vibration peak of NiFe LDH

542.0 cm^{-1}: [81]

1 Bridging type $[S_2]^{2-}$(ν(S-S)$_{br}$)

543.0 cm^{-1}: [58]

1 Vibration peak of Ni-O bond in NiOOH

545.0 cm^{-1}: [89,95]

1 Characteristic peaks of Ni_3N
2 Ni-O vibration in γ-NiOOH

548.0 cm^{-1}: [87]

1 Bending and stretching vibration of Co-O in CoOOH

549.0 cm^{-1}: [35,96]

1 The characteristic peaks of CoOOH
2 A_{1g} band of LNO

Continued on next page

550.0 cm^{-1}: [10,20,24,33,70,78,80,82,91]

1 Ni-O vibration in NiOOH
2 (Co/Fe) O (OH) structure
3 Fe and Ni species, such as α-FeOOH, α-Fe_2O_3, NiO (begin)
4 Oxygen defect related band
5 A_{1g} vibration mode of Mn-O nanosheets
6 CoII-O vibration
7 Boron (B) (begin)
8 The Raman spectra of molten NaF-AlF_3-Al_4C_3 salts
9 A_g vibrational modes of CoOOH species (end)

552.4 cm^{-1}: [62]

1 Metal-O Vibration in Metal-OOH

553.0 cm^{-1}: [9,80,96]

2 A_{1g}Ni-O stretching vibration mode in NiOOH
3 A_{1g} band of LNO

554.0 cm^{-1}: [29,98,101,114]

1 NiOOH
2 Formation of Ni(III)OOH on the surface of $NiCo_2O_4$
3 Polarized A_{1g} mode (stretching) of Ni^{III}-O
4 A_{1g} stretching mode of γ-NiOOH

555.0 cm^{-1}: [28,65,99]

1 Ni-O vibration of NiOOH
2 Polarized A_{1g} stretching mode of Ni-O(H) in NiOOH
3 High valence Nickel iron hydroxide (NiFe)OOH

556.0 cm^{-1}: [25,84,86]

1 Active NiOOH species (β-NiOOH)
2 Ni-OOH vibration
3 A_{1g}, Ni-O stretching vibration mode of γ-NiOOH
4 γ-NiOOH

558.0 cm^{-1}: [43,100]

1 Ni-O of γ-NiOOH phase
2 Polarized A_{1g} mode of γ-NiOOH (stretching vibration of oxygen atoms perpendicular to the plane)

560.0 cm^{-1}: [62,66,103,104]

1 Ni(III)-O stretching vibration (ν) modes in NiOOH
2 Depolarized E_g mode (bending) of NiIII-O in NiOOH
3 H_2SO_4 electrolyte
4 Characteristic Raman peaks of γ-NiOOH phase

561.0 cm^{-1}: [30]

1 NiOOH species

564.0 cm^{-1}: [105]

1 Typical extension of NiOOH (NiIII-O)

565.0 cm^{-1}: [30]

1 Tensile Vibration of Ni^{3+}-O
2 NiOOH species

566.0 cm^{-1}: [59,101]

1 In-plane stretching vibration of octahedral layers in δ-MnO_2
2 Peak value of NiFeLDH system

Continued on next page

568.0 cm^{-1}: [4]
1 Peaks of oxygen vacancies in Pd/ZnO_{100} samples

569.0 cm^{-1}: [35]
1 The characteristic peaks of CoOOH

570.0 cm^{-1}: [20]
1 Formation of Li_2O

571.0 cm^{-1}: [115]
1 Formation of Co-OH on $Co_2V_2O_7$ and Co_3O_4

573.0 cm^{-1}: [41,58]
1 Tensile vibration of A_g-Co-OH
2 Active CoOOH intermediate species

574.0 cm^{-1}: [90]
1 MnO lattice vibration of the basal plane of the MnO_2 sheets

575.0 cm^{-1}: [54]
1 In-plane MnO stretching

577.0 cm^{-1}: [90,107]
1 FeOOH
2 MnO lattice vibration of the basal plane of the MnO_2 sheets

579.0 cm^{-1}: [92]
1 The peak of MnO_2

580.0 cm^{-1}: [35,61,85]
1 Oxygen vacancies creation because of the entry of CeO_2 into the lattice of CuO (end)
2 ν(O-Ag-O) in surface and subsurface oxygen motifs
3 The characteristic peak of CoO_2

581.0 cm^{-1}: [56]
1 Peak of MoO_{3-x}($0<x<1$)

589.0 cm^{-1}: [4,73]
1 E_{1L} of ZnO_{100}
2 The vibration mode of Ni-O in Ni-OH

596.0 cm^{-1}: [79]
1 The stretching vibration of the M-O bond, suggesting the presence of a layered metal hydroxide phase

598.0 cm^{-1}: [37,40]
1
2 (D) mode caused by defects in CeO_2

600.0 cm^{-1}: [15,24,45,80,85,102,109]
1 Amorphous cobalt oxide
2 Formation of CoOOH
3 Oxygen vacancy of Fe2O3
4 corundum
5 Fe and Ni species, such as α-FeOOH, α-Fe_2O_3, NiO (end)
6 The E_g mode of $Co(OH)_2$
7 Co(Zn)OOH

601.0 cm^{-1}: [30]
1 Cu^{III}

604.0 cm^{-1}: [36]
1 A_{1g} vibration mode of anatase TiO_2

Continued on next page

605.0 cm^{-1}: [72,106]
1 Symmetric stretching of the bridging SiOSi in SiO_2
2 SiOSi symmetrical stretching of SiO_2

606.0 cm^{-1}: [35]
1 The characteristic peaks of CoOOH

608.0 cm^{-1}: [24]
1 $Co(OH)_2$-phase

610.0 cm^{-1}: [85,101]
1 Oxygen vacancies creation because of the entry of CeO_2 into the lattice of CuO (begin)
2 Formation of β-FeOOH

612.0 cm^{-1}: [35,69,97]
1 C-H bond of 4-NP and 4-AP
2 Lattice vibrations of Mo-O bonds
3 The characteristic peaks of CoOOH
4 Ce-O stretching mode

613.0 cm^{-1}: [12,116]
1 Vibration modes of specific bonds in R6G on cavity-based particle-in-quasicavity(PIQC) ZnO
2 A_{1g} vibration mode of anatase TiO_2

614.0 cm^{-1}: [35]
1 The characteristic peaks of CoOOH

614.8 cm^{-1}: [54]
1 MnO stretching of the MnOOH intermediate

615.0 cm^{-1}: [78]
1 The Raman spectra of molten NaF-AlF_3-Al_4C_3 salts

618.0 cm^{-1}: [32]
1 SO_3 species
2 SAg stretching

619.0 cm^{-1}: [13,22]
1 Surface Cu_2O (Cu_2O_{surf})
2 A_{1g} mode of nanocrystalline RuO_2

620.0 cm^{-1}: [67,70,106]
1 The vibration mode of Cu_2O
2 Stretching of symmetric oxygen cages of A_{2g}
3 Surface MnO_x oligomers
4 Grafting MnOSi bonds in MnO_x/SiO_2

620.3 cm^{-1}: [44]
1 B_g mode of CuO

621.0 cm^{-1}: [88,89]
1 F_{2g}-Co^{2+}-OH
2 Double degeneration into longitudinal optical mode of oxide, suggesting that abundant oxygen vacancies in CeO_2

623.0 cm^{-1}: [49,87]
1 Co-O vibration in NCMO
2 The vibration mode of anatase

624.0 cm^{-1}: [92]
1 The peak of MnO_2

Continued on next page

628.0 cm^{-1}: [113]
1 The vibration mode of Cu_2O

630.0 cm^{-1}: [59,90,114]
1 Out of plane symmetric stretching vibration of Mn-O in MnO_6
2 Presence of oxygen vacancies on NiGe film (end)
3 Symmetric stretching vibration of MnO band in MnO_6 octahedra

635.0 cm^{-1}: [30,58]
1 A_{1g} vibration of $NiCo_2O_4$
2 CuO

636.0 cm^{-1}: [110]
1 The E_g vibrational mode of Pd-O bonds

638.0 cm^{-1}: [12]
1 The E_g vibration mode of anatase TiO_2

643.0 cm^{-1}: [34,60]
1 Lepidocrocite (γ-FeOOH)
2 VCo/TiO stretching frequencies (along c axis) of STLC

645.0 cm^{-1}: [20,54,58,117]
1 The out-of-plane MnO stretching
2 A_{1g} vibration of $NiCo_2O_4$
3 second order of the LA (longitudinal acoustic) mode and the overtone of TA (transverse acoustic) and TO optical modes of a-Si
4 The vibrational modes of Pd-O bonds on Pd-based catalyst

650.0 cm^{-1}: [90]
1 Mn-O bonds of mixed valence manganese
2 Mn^{3+}/Mn^{4+}

660.0 cm^{-1}: [107,114]
1 Characteristic of vibrational modes directly involving Co species in MOFs catalyst
2 Presence of oxygen vacancies on NiGe film (begin)

663.0 cm^{-1}: [68]
1 $S_2O_3^{2-}$

665.0 cm^{-1}: [49]
1 Crystalline Cu_2O nanoparticles

667.0 cm^{-1}: [35]
1 Characteristic peaks of Co_3O_4

668.0 cm^{-1}: [118]
1 the bending out-of-plane mode of -CH, OH, and OC=O in MOF-AgNC(nanocube)

670.0 cm^{-1}: [82,98,119,120]
1 A_{1g} vibration mode of $NiCo_2O_4$
2 Octahedral-coordinated CoIIO stretch
3 CoII-O stretching vibration of Ag/iron oxide-doped NiO-CoO hollow spheres (FNCO-HSs)
4 Symmetric stretching modes of DMSO molecules
5 Guanine ring stretching vibration of single-stranded DNA

673.0 cm^{-1}: [97]
1 NO_2 bending of 4-NP

Continued on next page

675.0 cm^{-1}: [70]
1 Internal motion of oxygen within the $Co(Fe)O_6$ octahedra in the BSCF ($Ba_{0.5}Sr_{0.5}Co_{0.8}Fe_{0.2}O_3$-$\delta$) lattice

676.0 cm^{-1}: [106,110]
1 B_{1g} vibrational mode of Pd-O bond
2 Surface MnO_x oligomers

679.0 cm^{-1}: [120]
1 Guanine ring stretching vibration of duplex DNA

680.0 cm^{-1}: [20,22,26,35,61,66,115]
2 Typical Raman features of Ni-Fe-LDH
3 B_{2g} mode of nanocrystalline RuO_2
4 Vibration of Co_3O_4
5 Characteristic peaks of Co_3O_4
6 Boron (B) (end)
7 A_{1g} mode of CoO/rGO

684.0 cm^{-1}: [42]
1 NiO

685.0 cm^{-1}: [24,106]
1 A_{1g} mode of spinel Co_3O_4
2 Mn-O-Mn vibration of MnO_x-containing catalysts

686.0 cm^{-1}: [35]
1 Characteristic peaks of Co_3O_4

690.0 cm^{-1}: [85,91,109]
1 Co (II) - O vibration mode
2 T-vibration of Fe_2O_3
3 A_{1g} vibration mode of Co-O

694.0 cm^{-1}: [24]
1 A_{1g} vibrational modes of Co-O in octahedra

696.0 cm^{-1}: [88]
1 A_{1g}-Co^{3+}-O vibration

697.0 cm^{-1}: [121]
1 Symmetric stretching mode of O-W-O in WO_6 octahedra

698.0 cm^{-1}: [106]
1 Surface MnO_x oligomers

700.0 cm^{-1}: [50,55,64,94,101,119,120]
1 AuOH species at the surface
2 Surface hydroxyl species on Cu (CuOH)
3 Copper (hydrated) oxide peak (below 700)
4 Tensile vibration of Ni in nickel hydrate (begin)
5 Peak value of NiFeLDH system
6 Anti symmetric stretching mode of DMSO molecules
7 Silica framework vibrational modes (begin)

704.0 cm^{-1}: [38]
1 The stretching vibration of O-W-O

706.0 cm^{-1}: [67]
1 Cu-OH_{ad}

Continued on next page

710.0 cm^{-1}: [25,72,122]
1 The Fe-O bond of β-FeOOH
2 *O-O tensile vibration of OOH bridging adsorption structure
3 the WO_3 nanoparticles on the SiO_2 substrate

715.0 cm^{-1}: [78]
1 The characteristic peaks of $Na_3Al_3CF_8$

725.0 cm^{-1}: [72,101]
1 Small peak of β-FeOOH
2 ν_{as}W-O-W bridging mode

727.0 cm^{-1}: [120]
1 Adenine ring stretching vibration of single-stranded DNA

730.0 cm^{-1}: [71,120]
1 In plane bending vibrations (δCO_2^-)
2 Adenine ring stretching vibration of single-stranded DNA

737.0 cm^{-1}: [123]
1 The interaction between $Na_{1+x}V_3O_8$ and silicon oxide

740.0 cm^{-1}: [72]
1 ν_{as}W-O-W bridging mode

742.0 cm^{-1}: [124]
1 In-plane vibration mode of $*CO_2^-$

743.0 cm^{-1}: [125]
1 Ni (IV) - Oxo species

745.0 cm^{-1}: [120]
1 Thymine ring stretching vibration of single-stranded DNA

749.0 cm^{-1}: [120]
1 Thymine ring stretching vibration of single-stranded DNA

750.0 cm^{-1}: [126]
1 V-O-V (begin)

751.0 cm^{-1}: [56]
1 Peak of MoO_{3-x}($0<x<1$)

752.0 cm^{-1}: [60]
1 Co/TiO_6 octahedral rotation of STLC

753.0 cm^{-1}: [72]
1 W-O-W group

760.0 cm^{-1}: [59,123]
1 The stretching vibration mode of MnIV=O species
2 Mapping of $Na_{1+x}V_3O_8/SiO_2$ phase

761.0 cm^{-1}: [118]
1 Vibration of O-C=O

762.0 cm^{-1}: [90]
1 Carboxylate bending mode

765.0 cm^{-1}: [127]
1 υ(OOH*)

Continued on next page

770.0 cm^{-1}: [2]
1 Tetraglyme in the electrolyte

774.0 cm^{-1}: [116]
1 Vibration modes of specific bonds in R6G

779.0 cm^{-1}: [121]
1 Symmetric stretching mode of O-W-O in WO_6 octahedron

780.0 cm^{-1}: [126]
1 W-O-W

783.0 cm^{-1}: [112]
1 *O-O stretching vibration of OOH adsorption structure

784.0 cm^{-1}: [106,108]
1 V-O-Ag bonds in edge shared triangular bipyramids (V is five coordinated)
2 V-O-Ag bonds with different coordination structures in $Ag_{1.2}V_3O_8$
3 W-O vibration of WO_6 unit in Mn-WO_3

785.0 cm^{-1}: [119]
1 O-O stretching mode of Li_2O_2

788.0 cm^{-1}: [72]
1 Symmetric stretching of SiO_2 bridging Si-O-Si

790.0 cm^{-1}: [20]
1 $LiPF_6$

796.0 cm^{-1}: [72]
1 The combined vibration of ν_{as}(W-O-W) and ν_{as}(W-O-Pt)

800.0 cm^{-1}: [50,72,128]
1 The vibrational mode of adsorbed phosphate ions (begin)
2 Bridge W-O-W
3 Lateral Acoustic (TA) Branch of Graphite

802.0 cm^{-1}: [38]
1 The stretching vibration of O-W-O

804.0 cm^{-1}: [123,129]
1 νCu-H
2 V-O-V bonds bridge VO_5 and VO_6 units through co angular oxygen atoms

805.0 cm^{-1}: [49]
1 Crystalline WO_3

807.0 cm^{-1}: [130]
1 Bending vibration of outer ring C-H

808.0 cm^{-1}: [72]
1 the WO_3 nanoparticles on the SiO_2 substrate

810.0 cm^{-1}: [57,106]
1 Si-O-Si symmetric stretching of SiO_2
2 U(V) signal

811.0 cm^{-1}: [9,131]
1 SeO_3^{2-}
2 Crystalline Na_2WO_4 phase

Continued on next page

812.0 cm^{-1}: [132]
1 Surface bound peroxymonosulfate (PMS)

813.0 cm^{-1}: [112]
1 *O-O stretching vibration of OOH adsorption structure

815.0 cm^{-1}: [61,72,123]
1 ν(O-O) in surface atomic-molecular hybrid structure: Ag_2-O-O-Ag_2, ν(O-O) in surface Ag_4-O-O structure, ν(O-O) in molecular oxygen complex Ag_x-O-O stabilized by subsurface atomic oxygen
2 Mapping of $Na_{1+x}V_3O_8/SiO_2$ Phase
3 WOW

816.0 cm^{-1}: [133]
1 CH_3 shear vibration
2 dimethyl phthalate (DMP)

823.0 cm^{-1}: [134]
1 the vibrational mode of δC-H rocking of metronidazole (MNZ)

825.0 cm^{-1}: [103]
1 Mo-O stretching mode from MoO_4^{2-}

826.0 cm^{-1}: [53,133]
1 The stretching mode of the V-O
2 Characteristic peaks of interfering substance diisodecyl o-phthalate (DIDP) (+)

830.0 cm^{-1}: [41,126]
1 V-O-V (end)
2 Short symmetric V-O vibration (A_{1g} mode)

831.0 cm^{-1}: [40]
1 Stretching vibration of OO bonds of peroxo species (O_2^2)

832.0 cm^{-1}: [122,135]
1 $S_2O_8^{2-}$
2 The O-O stretching vibration frequency of peroxide species

834.0 cm^{-1}: [9,136]
1 SeO_4^{2-}
2 Ni-PMS*

836.0 cm^{-1}: [120]
1 PO_2^{-1} stretch

840.0 cm^{-1}: [74]
1 Stretching vibrational mode of the V-O

848.0 cm^{-1}: [47]
1 4,4-biphenyldicarboxylic ion ($Bpdc^{2-}$) ligand dissociated from MOFs

850.0 cm^{-1}: [94,114,115]
1 Tensile vibration of Ni in nickel hydrates (end)
2 Vibration of $Co_2V_2O_7$ caused by surface oxidation of VN
3 ν(O-O) of an active oxygen species ($NiOO^-$) in oxyhydroxide structure

851.0 cm^{-1}: [137]
1 The formation of O_{ad}*

Continued on next page

860.0 cm^{-1}: [49]
1 $CeVO_4$ nanoparticles

874.0 cm^{-1}: [106]
1 W-O vibration of WO_6 unit in $MnWO_4$

880.0 cm^{-1}: [61,125]
1 Reactive oxygen species
2 Stable molecular oxygen complex structure
3 Metastable PMS adsorbed species formed by PMS molecules (*HSO_5^-, NiN_4-PMS*)

882.0 cm^{-1}: [132]
1 SO_5^{2-}

884.0 cm^{-1}: [108]
1 V-O-Ag linkages in $AgVO_3$ (V is five-coordination)

885.0 cm^{-1}: [106]
1 Surface MnO_x oligomers

886.0 cm^{-1}: [87]
1 O-Mo-O stretching vibration in NiCoMo oxides (NCMO) phase

890.0 cm^{-1}: [2,49]
1 Tetraethyl ether
2 $Cu_xV_yO_z$ nanoparticles

900.0 cm^{-1}: [20,65]
1 NiO
2 EC and DEC solvents

908.0 cm^{-1}: [133]
1 interference diallyl phthalate (DAP) (-)

910.0 cm^{-1}: [49]
1 $CuWO_4$ nanoparticles

912.0 cm^{-1}: [27]
1 Asymmetric stretching of C_α-C_β

913.0 cm^{-1}: [103]
1 Mo-O stretching vibration mode of MoO_4^{2-}

915.0 cm^{-1}: [97,130]
1 Bending vibration of NO_2
2 Ring skeletal vibration of radial orientation

918.0 cm^{-1}: [107]
1 -CN

922.0 cm^{-1}: [108]
1 VOAg linkage in $Ag_{1.2}V_3O_8$
2 $VAgO_x/\alpha$-Al_2O_3

923.0 cm^{-1}: [39]
1 $Co(OH)_2$

926.0 cm^{-1}: [38]
1 Crystalline Na_2WO_4 phase

Continued on next page

927.0 cm^{-1}: [138]
1 Raman peaks of crystalline Na_2WO_4

928.0 cm^{-1}: [32]
1 SO_3 species

930.0 cm^{-1}: [49,119,139,140]
1 The vibrational modes of $\nu_{O\text{-}Cr\text{-}O}$ bonds
2 $Ce_2(WO_4)_3$ nanoparticles
3 Asymmetric modes of VO_2^+
4 Cl-O scaling mode of $LiClO_4$

933.0 cm^{-1}: [122,141]
1 $\nu_s(ClO_4^-)$
2 Symmetric stretching vibration mode of ClO_4^-

935.0 cm^{-1}: [140,142]
1 Perchlorate ion
2 Additional modes of VO_2HSO_4

936.0 cm^{-1}: [112]
1 Symmetric stretching mode of perchlorate ion (ClO_4^-)

937.0 cm^{-1}: [123]
1 β-$NaVO_3$ species (begin)

942.0 cm^{-1}: [106,123]
1 β-$NaVO_3$ species (end)
2 W=O stretching vibration of isolated Na-WO_4 surface sites

945.0 cm^{-1}: [123]
1 VO_2 symmetric stretching of crystal state β-$NaVO_3$

950.0 cm^{-1}: [131,138]
1 W=O bond in WO_4 (F) unit
2 Raman peaks of Na-WO_4

958.0 cm^{-1}: [32,72]
1 SO_4 species
2 ν_s(W=O) vibration of bridging W

960.0 cm^{-1}: [72]
1 ν_s(W=O) vibration of bridging W

970.0 cm^{-1}: [38,106]
1 The peak of W=O bond
2 SiOH stretching mode of the surface hydroxyls

973.0 cm^{-1}: [72]
1 ν_s(W=O) vibration of terminal W

975.0 cm^{-1}: [72,143]
1 ReO_4^-
2 Terminal SiOH vibration
3 Terminal W=O bands

977.0 cm^{-1}: [72]
1 W1/SiO_2

979.0 cm^{-1}: [59,132]
1 SO_4^{2-}

Continued on next page

980.0 cm^{-1}: [15,72,144]
1 Vibration of SO_4^{2-} ion
2 Na_2SO_4
3 W4/SiO_2
4 ν_s(W=O) vibration of terminal W

981.0 cm^{-1}: [138,145]
1 Sulfate radical species
2 Mn-WO_4

982.0 cm^{-1}: [125,136]
1 SO_4^{2-}

985.0 cm^{-1}: [138]
1 WO_4 species

986.0 cm^{-1}: [88]
1 NiOOH peak

988.0 cm^{-1}: [59]
1 Symmetric stretching vibrational mode of PO_3 in HPO_4^{2-}

990.0 cm^{-1}: [140,146]
1 Reduced form of PPy (CC ring deformation)
2 V=O stretching vibration

992.0 cm^{-1}: [123]
1 V=O stretching vibration in VO_5 polyhedra

993.0 cm^{-1}: [68]
1 $S_2O_3^{2-}$

995.0 cm^{-1}: [143]
1 Re-O-Ti vibration of isolated four coordinated rhenium oxide monomers

996.0 cm^{-1}: [27]
1 The ring-breathing mode of the phenyl groups in the $[AlPh_4]^-$ anions

997.0 cm^{-1}: [49]
1 Crystalline V_2O_5

998.0 cm^{-1}: [147]
1 In plane bending of benzene ring in TP molecule (δ-CCC)
2 Benzol Toroidal Bend (δ-CCC) in PMBA Molecules

1000.0 cm^{-1}: [120,143]
1 Re-O-Ti of isolated four coordinated rhenium oxide monomers
2 Silica framework vibrational modes (end)

1003.0 cm^{-1}: [120]
1 Phenyl ring breathing

1007.0 cm^{-1}: [135]
1 SO_4^{2-}

1010.0 cm^{-1}: [73,128]
1 Superoxide (O-O) species adsorbed on the surface of high-entropy alloy (HEA)
2 Symmetric C-O stretching vibration of HCO_3^-

Continued on next page

1012.0 cm^{-1}: [49]
1 Raman peaks of surface WO_x on TiO_2 support

1014.0 cm^{-1}: [48]
1 Bicarbonate

1015.0 cm^{-1}: [137,138,148]
1 CO_2^{2-} adsorbed on electrode surface in electrolyte
2 Formation of O_2*
3 W=O bond in WO_x mono-oxo species

1022.0 cm^{-1}: [147]
1 CH in-plane bending (δ_{CH})

1025.0 cm^{-1}: [143]
1 Surface sulfate

1026.0 cm^{-1}: [105,149]
1 C-O bonds of methylol groups
2 MeOH

1027.0 cm^{-1}: [142]
1 Stretching of linear dimers and/or high polymers

1028.0 cm^{-1}: [27,58]
1 C_α - C_β symmetric stretching
2 The A_{1g} mode of Ni-O in $NiCo_2O_4$

1029.0 cm^{-1}: [110]
1 α-NiH vibration mode

1030.0 cm^{-1}: [49,79,119]
1 Vibration of pyridine ring
2 Raman peaks of surface VO_x on TiO_2 support
3 CH_3 rocking mode

1035.0 cm^{-1}: [140,142]
1 ν(S=O)
2 $HSO_4^-..H_3O^+$ sulfur oxygen bond stretching vibration

1039.0 cm^{-1}: [123]
1 Isolation vanadium oxo (V=O) in $[VO_4]/SiO_{2(500\text{-air})}$

1040.0 cm^{-1}: [142]
1 In-phase S=O stretching mode

1041.0 cm^{-1}: [127]
1 υ(OH*)

1044.0 cm^{-1}: [32]
1 SO_4 species

1046.0 cm^{-1}: [32]
1 NO_3 species

1047.0 cm^{-1}: [88,140,144]
1 The formation of O* on the Co sties (C-O*)
2 Stretching of NO_3^-
3 HSO_4^-

1050.0 cm^{-1}: [62,146,150]
1 H_2SO_4 electrolyte
2 C-H in-plane deformation in neutral PPy units
3 NO_3^- ion

Continued on next page

1051.0 cm^{-1}: [42,142]
1 Out-of-phase S=O stretching mode
2 Ni oxide NiO

1054.0 cm^{-1}: [34]
1 Lepidocrocite (γ-FeOOH)

1057.0 cm^{-1}: [73]
1 Symmetric stretching vibration mode of SO_4^{2-}

1059.0 cm^{-1}: [132]
1 SO_5^{2-}

1060.0 cm^{-1}: [136]
1 Vibration mode of HSO_5^-

1062.0 cm^{-1}: [110,125]
1 $2P_{LO}$ of NiO vibrational modes
2 HSO_5^-

1064.0 cm^{-1}: [88,101,151]
1 Active oxygen species (O*) at the Ni sites
2 C-O stretching vibration of CO_3^{2-}
3 Carbonate ions inserted into D-NiFeAlLDH

1065.0 cm^{-1}: [55]
1 Adsorbed carbonate

1069.0 cm^{-1}: [48]
1 Carbonate

1071.0 cm^{-1}: [147,152]
1 In plane bending and C-S stretching of benzene ring in p-mercaptobenzoic acid (PMBA) molecules ($\delta_{CCC}+\gamma_{CS}$)
2 C-S vibration (δ_{CS})
3 Aromatic ring breathing, symmetric C-H plane bending and C-S extension

1072.0 cm^{-1}: [105]
1 [O-O] Vibration

1073.0 cm^{-1}: [122]
1 *OH species in Pt_3Co@Pt-SAC

1074.0 cm^{-1}: [135]
1 $S_2O_8^{2-}$

1077.0 cm^{-1}: [130]
1 Peak value of 4-aminothiophenol (4-ATP)

1080.0 cm^{-1}: [146,153]
1 4-ATP
2 C-H in-plane deformation in polarons

1083.0 cm^{-1}: [154]
1 C-S vibration in p-nitrothiophenol (PNTP) and DMAB

1084.0 cm^{-1}: [130]
1 C-S telescopic vibration

1087.0 cm^{-1}: [79]
1 Surface OOH* intermediate

Continued on next page

1090.0 cm^{-1}: [65]
1 NiO

1094.0 cm^{-1}: [143]
1 v_{asym}(S-O) of surface sulfates

1100.0 cm^{-1}: [20,50,120]
1 The vibrational mode of adsorbed phosphate ions (end)
2 Li_2CO_3
3 C-H mode

1120.0 cm^{-1}: [90]
1 Vibration of $\upsilon_{C\text{-}O}$ and $\delta_{c\text{-}O\text{-}H}$

1124.0 cm^{-1}: [124]
1 Symmetric stretching mode of $*CO_2^-$

1130.0 cm^{-1}: [44]
1 Multi phonon (MP) transition mode of CuO

1139.0 cm^{-1}: [150,155]
1 Head-to-Head Coupling Product p,p-dimercaptoazobenzene (DMAB)
2 $-NH_2$

1144.0 cm^{-1}: [130]
1 C-N symmetric stretching

1150.0 cm^{-1}: [143]
1 Surface sulfate on the catalyst

1152.0 cm^{-1}: [156]
1 $-NH_2$

1158.0 cm^{-1}: [118]
1 CH wagging of $HCOO^-$

1160.0 cm^{-1}: [148]
1 Symmetric stretching vibration of $*CO_2^-$ ($v_sCO_2^-$)

1161.0 cm^{-1}: [157]
1 In-plane C-H bending

1170.0 cm^{-1}: [33]
1 2LO overtone

1174.0 cm^{-1}: [37]
1 Second order longitudinal mode of CeO_2 lattice (2LO)

1178.0 cm^{-1}: [130]
1 In-plane ring CH bending

1180.0 cm^{-1}: [40]
1 The second-order longitudinal optical mode of the fcc fluorite phase of CeO_2

1181.0 cm^{-1}: [158]
1 Bending vibration mode of C-H stretching vibration

1188.0 cm^{-1}: [134]
1 The in-plane bending mode of metronidazole (MNZ) molecules

Continued on next page

1200.0 cm^{-1}: [94,107,114]
1 -OH (begin)
2 Tensile vibration of nickel in nickel hydrates
3 Vibration of reactive oxygen species ($NiOO^-$) in the structure of oxygen hydrides

1220.0 cm^{-1}: [159]
1 Disordered graphite lattice with A_{1g} symmetry

1221.0 cm^{-1}: [157]
1 C-N stretching

1225.0 cm^{-1}: [155]
1 Head-to-tail coupling product 4-mercapto-N-phenylquinone diimine (NPQD)

1227.0 cm^{-1}: [118]
1 The stretching vibrational mode of CO and rocking mode of -CH

1240.0 cm^{-1}: [120]
1 Thymine pattern

1250.0 cm^{-1}: [33]
1 The presence of the salt form of flexible-chain PAMPSA

1255.0 cm^{-1}: [146]
1 The presence of the salt form of flexible-chain PAMPSA

1257.0 cm^{-1}: [120]
1 Amide III stretching mode

1270.0 cm^{-1}: [118]
1 Fermi resonance of CO_2 and -CH rocking vibration of MOF-801

1280.0 cm^{-1}: [47]
1 $Bpdc^{2-}$ ligand dissociated from MOFs

1283.0 cm^{-1}: [58,134]
1 Twisting of MNZ molecule
2 Symmetric tensile vibration of C-O

1288.0 cm^{-1}: [124]
1 OH- deformation in *COOH

1290.0 cm^{-1}: [160]
1 $-NO_2$ peak

1300.0 cm^{-1}: [34,107,130]
1 Ring C-C stretching vibration
2 Lepidocrocite (γ-FeOOH)
3 -OH (end)

1308.0 cm^{-1}: [129]
1 Stretching vibration ($v_sCO_2^-$)

1310.0 cm^{-1}: [15]
1 Hematite

1317.0 cm^{-1}: [73]
1 D-bands in carbon nanofibers (CNFs)

Continued on next page

1320.0 cm^{-1}: [75,159]
1 Disordered graphite lattice with A_{1g} symmetry
2 Amorphous layer of C@ZnO sample

1330.0 cm^{-1}: [160]
1 Adsorption on Au-2

1333.0 cm^{-1}: [130]
1 O-N-O stretching vibration

1335.0 cm^{-1}: [3,119,144]
1 Graphitic carbon (D band)
2 Stretching vibration of N=O in NO_2^-
3 D-bands related to lattice structure defects in carbon materials

1336.0 cm^{-1}: [97]
1 Bending vibration of NO_2

1337.0 cm^{-1}: [12]
1 sp^3 disordered carbon in TiO_2-CNT (carbon nanotube) film

1340.0 cm^{-1}: [19,127,149,160]
1 C-H bonds of methylol groups
2 $\nu(NO_2)$
3 Vibration modes of disordered carbon (D)
4 Structural defects in graphene (D-band)

1342.0 cm^{-1}: [54]
1 O-O stretching and contraction of Mn-OOD

1344.2 cm^{-1}: [161]
1 D peak of C-C (related to defects)

1346.0 cm^{-1}: [1]
1 D-band of graphite

1347.0 cm^{-1}: [58]
1 Water bending

1350.0 cm^{-1}: [20,54,90,162]
1 Breathing patterns of *K*-point A_{1g} phonons
2 Structural defects of graphite electrodes
3 Breathing modes of sp^2 hexagonal ring in multilayer graphene foam
4 Carboxyl group

1352.0 cm^{-1}: [162]
1 Defects in carbon fiber structure

1354.0 cm^{-1}: [54]
1 O-O stretching vibration of Mn-OOH intermediate

1360.0 cm^{-1}: [63]
1 D-band of organic matrix
2 G-band of carbon nanotubes

1364.0 cm^{-1}: [116]
1 Vibration modes of specific bonds in R6G

1370.0 cm^{-1}: [160]
1 $-NO_2$ peak

Continued on next page

1375.0 cm^{-1}: [144]
1 $-NH_2$ bending vibration

1389.0 cm^{-1}: [163]
1 C=N bonds in organic ligands of MOFs

1390.0 cm^{-1}: [160]
1 Azo group of DMAB

1391.0 cm^{-1}: [130]
1 N-N stretching

1395.0 cm^{-1}: [158]
1 Vibration of $C=C_{wing}$

1411.0 cm^{-1}: [144]
1 The NO_2 stretching of NO_3^-

1416.0 cm^{-1}: [79]
1 In- and out-of-phase stretching modes of the carboxylate group

1420.0 cm^{-1}: [107]
1 COOH functional group

1422.0 cm^{-1}: [124]
1 Symmetric extension of $*CO_2^-$

1426.0 cm^{-1}: [142]
1 δ(C-H) mode

1435.0 cm^{-1}: [130]
1 C-H in-plane bending mode

1438.0 cm^{-1}: [118]
1 Vibration of O-C=O

1440.0 cm^{-1}: [160]
1 azo group of DMAB

1441.0 cm^{-1}: [154]
1 N=N vibration in DMAB

1442.0 cm^{-1}: [155]
1 Head-to-head coupling product DMAB

1445.0 cm^{-1}: [34,133]
1 Methylene deformation mode (δCH_2)
2 CH_3 shear vibration
3 di(2-ethylhexyl) phthalate (DEHP)

1450.0 cm^{-1}: [20,118]
1 CH_2 scissoring of polystyrene (PS)
2 Amorphous carbon

1452.0 cm^{-1}: [150]
1 Asymmetric bending vibration of NH_4^+

1482.0 cm^{-1}: [157]
1 C=N stretching of quinone (Q)

1490.0 cm^{-1}: [155]
1 Head-to-tail coupling product NPQD

Continued on next page

1500.0 cm^{-1}: [120,159]
1 The presence of amorphous carbon
2 C-C mode

1510.0 cm^{-1}: [35]
1 $C=C_{ring}$ in DFF

1515.0 cm^{-1}: [35]
1 $C=C_{ring}$ in HMFCA

1517.0 cm^{-1}: [30]
1 The disappearance of $C=C_{ring}$ vibration mode in 2,5-furandicarboxylic acid (FDCA)

1518.0 cm^{-1}: [35]
1 $C=C_{ring}$ in FDCA

1523.0 cm^{-1}: [30,35]
1 C=C ring in 5-hydroxymethylfurfural (HMF) molecules

1525.0 cm^{-1}: [145]
1 Vibration of -NH bonds

1526.0 cm^{-1}: [156]
1 -NH

1528.0 cm^{-1}: [35,150]
1 $C=C_{ring}$ in FDCA
2 -NH
3 Adsorbed H_2NOH

1538.0 cm^{-1}: [120,130]
1 Ring C-C stretching vibration
2 Amide II stretching mode

1540.0 cm^{-1}: [129,148]
1 Asymmetric stretching vibration of $*CO_2^-$ ($\nu_{as}CO_2^-$)

1547.0 cm^{-1}: [129]
1 $\nu_{as}CO_2^-$

1550.0 cm^{-1}: [118]
1 The O=C=O asymmetric vibration of CO_2 and stretching vibration of polystyrene (PS)

1570.0 cm^{-1}: [130]
1 Phenyl ring mode

1577.0 cm^{-1}: [147,164]
1 C-C stretching mode (γ_{cc})
2 The stretching of the in-plane CC bonds

1579.0 cm^{-1}: [165]
1 In-plane vibration of sp^2 carbon atoms in graphite

1580.0 cm^{-1}: [3,166]
1 Graphitic carbon (G band)
2 The G-band of N-doped porous carbon matrix (NDPCM)

1581.0 cm^{-1}: [127,152]
1 Aromatic C-C extension, asymmetric C-H in-plane bending
2 Graphene carbon (G)

Continued on next page

1581.2 cm^{-1}: [19]
1 Ordered sp^2 bonded carbon (G-band) of graphene

1581.9 cm^{-1}: [161]
1 G peak of C-C (related to graphitic carbon)

1582.0 cm^{-1}: [147]
1 C-C stretching mode (γ_{cc})

1585.0 cm^{-1}: [12]
1 Sp^2 bonded carbon atoms in TiO_2-CNT films

1587.0 cm^{-1}: [130]
1 Ring C-C stretching vibration

1590.0 cm^{-1}: [19,20,71,79,90,159,160]
1 The in- and out-of-phase stretching modes of the carboxylate group
2 Ring vibration of defect free graphite lattice (E_{2g} symmetry)
3 The stretching vibration of $-NH_2$ groups
4 Ordered sp^2 bonded carbon (G-band) of graphene
5 G band related to sp^2-linke carbon atoms in uncoated graphite electrodes
6 High-frequency bond stretching of sp^2 carbon pairs in rings and chains
7 Adsorbed carboxyl species ($*CO_2^-$)

1592.0 cm^{-1}: [167]
1 Characteristic peaks of 4-mercapto-benzonitrile (4-MBN) molecules

1593.0 cm^{-1}: [130,164]
1 Peak value of 4-ATP
2 The stretching of the in-plane CC bonds

1596.0 cm^{-1}: [97,162]
1 G-bands of CFP, CCFC, and FCFC
2 Crystallinity in Carbon Fiber Structure

1597.0 cm^{-1}: [146]
1 C=C stretching in the oxidized pyrrole ring

1598.0 cm^{-1}: [116]
1 Vibration modes of specific bonds in 3,3',4,4-tetrachlorobiphenyl (one congener of polychlorinated biphenyls, PCB-77)

1600.0 cm^{-1}: [47,166,168]
1 $Bpdc^{2-}$ ligand dissociated from MOFs
2 C=C vibration
3 Peak of H_2O

1601.0 cm^{-1}: [58]
1 The bending vibration of water

1605.0 cm^{-1}: [54]
1 The G band of the E_{2g} phonon of sp^2 carbons

1606.0 cm^{-1}: [169]
1 HOH bending of water

Continued on next page

1607.0 cm^{-1}: [120]
1 C=C stretching modes

1608.0 cm^{-1}: [73]
1 G-band in CNFs

1609.0 cm^{-1}: [158]
1 Vibration mode of $C=C_{ring}$

1610.0 cm^{-1}: [162]
1 benzene ring

1612.0 cm^{-1}: [120]
1 C=C stretching peak

1617.0 cm^{-1}: [163]
1 C=C Bond in Organic Ligands of MOFs

1620.0 cm^{-1}: [130,159,170]
1 Ring C-C stretching vibration
2 ν_{IP} (Aromatic C-C)
3 the presence of a poorly ordered graphite structure

1632.0 cm^{-1}: [150]
1 Adsorbed H_2NOH

1637.0 cm^{-1}: [77]
1 α-$Ni(OH)_2$

1638.0 cm^{-1}: [129]
1 δH_2O

1639.0 cm^{-1}: [155]
1 Head-to-tail coupling product NPQD

1639.4 cm^{-1}: [171]
1 Bending vibration of H-OH bonds

1640.0 cm^{-1}: [94,120]
1 Vibration of water molecules
2 The bending vibration mode of water

1642.0 cm^{-1}: [118,133]
1 the C=O vibration/OH rocking of HOCO*
2 Characteristic peaks of interfering substance diallyl phthalate (DAP)

1643.1 cm^{-1}: [171]
1 Bending vibration of H-OH bonds

1650.0 cm^{-1}: [34]
1 The bending mode of NH groups

1661.0 cm^{-1}: [30,118]
1 Vibration of C=C
2 Aldehyde groups of HMF molecules

1664.0 cm^{-1}: [149]
1 C=O bond of aldehyde group

1668.0 cm^{-1}: [120]
1 The carbonyl stretching vibration of thymine, guanine, and cytosine

Continued on next page

1669.0 cm^{-1}: [30]
1 The peak associated with aldehyde oxidation

1727.0 cm^{-1}: [90]
1 $\upsilon_{C=O}$

1750.0 cm^{-1}: [166]
1 Peak of H_3O^+

1780.0 cm^{-1}: [120]
1 The stretching vibration peak of thiosuccinimide

1800.0 cm^{-1}: [48,67]
1 Stretching of C≡O
2 *CO on hollow sites (begin)

1860.0 cm^{-1}: [172]
1 C≡O tensile vibration of CO (CO_{bridge})

1900.0 cm^{-1}: [67]
1 *CO on bridge sites (begin)
2 *CO on hollow sites (end)

1939.0 cm^{-1}: [44]
1 Adsorbed *CO intermediates on the CuO@C-600 electrode

1980.0 cm^{-1}: [113]
1 Interactions between CO* intermediates

1998.0 cm^{-1}: [173]
1 CO_{bridge} on Cu_2O-TiO_2 interface

2000.0 cm^{-1}: [67,174]
1 C≡O stretching of *CO (begin)
2 *CO on top sites (linearly *CO) (begin)
3 *CO on bridge sites (end)

2010.0 cm^{-1}: [129]
1 $\nu_s CO$

2056.0 cm^{-1}: [128]
1 Expansion and contraction vibration of C=O

2070.0 cm^{-1}: [113]
1 C-O stretching vibrational mode of absorbed *CO on a Cu top site ($*CO_{atop}$)

2085.0 cm^{-1}: [129]
1 νC≡O

2100.0 cm^{-1}: [48]
1 Stretching of C≡O

2120.0 cm^{-1}: [67,173]
1 *CO on top sites (linearly *CO) (end)
2 CO_{atop} on Cu_2O-TiO_2 Interface

2180.0 cm^{-1}: [175]
1 The characteristic peak of cyanide bridge (C≡N)

2200.0 cm^{-1}: [174]
1 C≡O stretching of *CO (end)

Continued on next page

2208.0 cm^{-1}: [158]
1 The vibration mode of C≡N

2230.0 cm^{-1}: [167]
1 Characteristic peaks of 4-MBN molecules

2530.0 cm^{-1}: [127]
1 υ(S-H)

2532.0 cm^{-1}: [141]
1 Stretching vibration of S-H, v(S-H)

2541.0 cm^{-1}: [107]
1 $-CH_3$

2550.0 cm^{-1}: [176]
1 O-D vibration

2580.0 cm^{-1}: [120]
1 The distinctive thiol SH stretching mode

2670.0 cm^{-1}: [127]
1 Vibration modes of 2D layers

2677.0 cm^{-1}: [1]
1 2D bands of graphite

2700.0 cm^{-1}: [90]
1 D peak related to the number of graphene layers and orientation

2800.0 cm^{-1}: [34]
1 Antisymmetric ($\nu_s CH_2$) stretching mode of methylene groups

2848.0 cm^{-1}: [67]
1 Intermediate products $-CH_x$ in CO_2RR

2874.0 cm^{-1}: [67]
1 Intermediate products $-CH_x$ in CO_2RR

2900.0 cm^{-1}: [177]
1 metal-OH band of OH*

2904.0 cm^{-1}: [67]
1 Intermediate products $-CH_x$ in CO_2RR

2934.0 cm^{-1}: [168]
1 C-H vibration

2936.0 cm^{-1}: [67]
1 Intermediate products $-CH_x$ in CO_2RR

2961.0 cm^{-1}: [67]
1 Intermediate products $-CH_x$ in CO_2RR

3000.0 cm^{-1}: [34,90]
1 Antisymmetric ($\nu_a CH_2$) stretching mode of methylene groups
2 O-H stretching of hydroxyl groups

Continued on next page

3004.0 cm^{-1}: [34]
1 The ethylenic elongation (νCH(C=C))

3200.0 cm^{-1}: [174,176,177]
1 Tetrahedrally coordinated H-bonded water
2 Raman peaks of interfacial water
3 O-H vibration

3400.0 cm^{-1}: [174,176]
1 Trihedrally coordinated H-bonded water
2 O-H vibration

3458.0 cm^{-1}: [169]
1 OH stretching mode of water

3500.0 cm^{-1}: [90,177]
1 Raman peaks of interfacial water
2 O-H stretching of COOH groups

3600.0 cm^{-1}: [174]
1 The H-bonding-free water with the dangling OH bonds

Scheme of oFDTD

1. **Simulation Software:** The FDTD simulation is conducted using ANSYS Lumerical FDTD 2020 R2.4.
2. **Simulation Objects:** The objects under simulation include a silicon wafer and two metallic particles made of noble metal (Fe, Co, Ni, Cu, Rh, Pd, Ag, Os, Lr, Pt, Au).

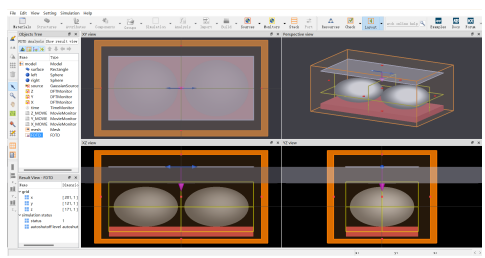

The diatomic FDTD simulation model

Table 1 Noble Metals Used in Diatomic FDTD Simulation Model

Metal	Optical Constants Source
Fe	Fe (Iron) - Palik
Co	n: 2.5769, k: 4.6527 [178,179]
Ni	Ni (Nickel) - Palik
Cu	Cu (Copper) - Palik
Rh	Rh (Rhodium) - Palik
Pd	Pd (Palladium) - Palik
Ag	Ag (Silver) - Johnson and Christy
Os	n: 4.2664, k: 3.25 [178,180]
Ir	n: 2.4852, k: 4.9865 [178,181]
Pt	Pt (Platinum) - Palik
Au	Au (Gold) - Johnson and Christy

3. **Silicon Wafer Specifications:** The silicon wafer measures 90nm in length, 45nm in width, and 10nm in height.

4. **Metallic Particles Specifications:** Each metallic particle has a radius of 20nm.

5. **Light Source:** A Gaussian light source with an amplitude of 1 is employed.

6. **Wavelength:** The simulation operates at a central wavelength of 532nm and 785nm with a wavelength span of 300nm.

7. **Monitor Setup:** The simulation monitors the X, Y, and Z cross-section along the axis defined by the line connecting the centers of the two metallic particles, and exports the data for further analysis.

8. **Mesh Size:** The maximum mesh step sizes, dx, dy, and dz, are set to 0.5nm to ensure accurate simulation results.

9. **FDTD Region:** The FDTD computational region encompasses all objects within a size of 100nm by 60nm by 85nm.

References

1 L. Qiao, C. Wang and X. S. Zhao, *ACS Applied Energy Materials*, 2021, **4**, 7012–7019.

2 T. Yamanaka, A. C. Kucuk, Z. Ogumi and T. Abe, *ACS Applied Energy Materials*, 2020, **3**, 9390–9400.

3 W. Yao, C. Tian, C. Yang, J. Xu, Y. Meng, I. Manke, N. Chen, Z. Wu, L. Zhan, Y. Wang and R. Chen, *Advanced Materials*, 2022, **34**, 2106370.

4 J. Gao, B. Wu, C. Cao, Z. Zhan, W. Ma and X. Wang, *ACS Sustainable Chemistry & Engineering*, 2021, **9**, 6370–6379.

5 G. Chen, Y. Kang, H. Yang, M. Zhang, J. Yang, Z. Lv, Q. Wu, P. Lin, Y. Yang and J. Zhao, *Advanced Functional Materials*, 2023, **33**, 2300656.

6 L. Ma, G. Zhu, Z. Wang, A. Zhu, K. Wu, B. Peng, J. Xu, D. Wang and Z. Jin, *Nano Letters*, 2023, **23**, 5272–5280.

7 C. Prehal, H. Fitzek, G. Kothleitner, V. Presser, B. Gollas, S. A. Freunberger and Q. Abbas, *Nature Communications*, 2020, **11**, 4838.

8 S.-C. Wu, Y. Ai, Y.-Z. Chen, K. Wang, T.-Y. Yang, H.-J. Liao, T.-Y. Su, S.-Y. Tang, C.-W. Chen, D. C. Wu, Y.-C. Wang, A. Manikandan, Y.-C. Shih, L. Lee and Y.-L. Chueh, *ACS applied materials & interfaces*, 2020, **12**, 27064–27073.

9 H. Zhang, X. He, K. Dong, Y. Yao, S. Sun, M. Zhang, M. Yue, C. Yang, D. Zheng, Q. Liu, Y. Luo, B. Ying, S. Alfaifi, X. Ji, B. Tang and X. Sun, *Materials Today Physics*, 2023, **38**, 101249.

10 Y. Li, Y. Duan, K. Zhang and W. Yu, *Chemical Engineering Journal*, 2022, **433**, 134472.

11 R. Belgamwar, R. Verma, T. Das, S. Chakraborty, P. Sarawade and V. Polshettiwar, *Journal of the American Chemical Society*, 2023, **145**, 8634–8646.

12 J. Li, J. Ao, C. Zhong and T. Yin, *Applied Surface Science*, 2021, **563**, 150301.

13 M. He, X. Chang, T.-H. Chao, C. Li, W. A. Goddard, M.-J. Cheng, B. Xu and Q. Lu, *ACS Catalysis*, 2022, **12**, 6036–6046.

14 B. Yu, A. Huang, K. Srinivas, X. Zhang, F. Ma, X. Wang, D. Chen, B. Wang, W. Zhang, Z. Wang, J. He and Y. Chen, *ACS Nano*, 2021, **15**, 13279–13288.

15 W. Zhang, D. Young, B. Brown, C. Shafer, F. Lu, E. Anyanwu and M. Singer, *Corrosion Science*, 2021, **188**, 109516.

16 Z. Cheng, M. Wang, Y. Dong, Y. Han, X. Yan, L. Xie, X. Zheng, L. Han and J. Zhang, *Journal of Colloid and Interface Science*, 2023, **649**, 86–96.

17 J. Xia, W. Hua, L. Wang, Y. Sun, C. Geng, C. Zhang, W. Wang, Y. Wan and Q.-H. Yang, *Advanced Functional Materials*, 2021, **31**, 2101980.

18 Q. Zeng, X. Li, W. Gong, S. Guo, Y. Ouyang, D. Li, Y. Xiao, C. Tan, L. Xie, H. Lu, Q. Zhang and S. Huang, *Advanced Energy Materials*, 2022, **12**, 2104074.

19 J. Zhang, Q. Zhang, X. Qu, G. Xu, B. Fan, Z. Yan, F. Gui and L. Yang, *Applied Surface Science*, 2022, **574**, 151559.

20 G. Elomari, L. Hdidou, H. Larhlimi, M. Aqil, M. Makha, J. Alami and M. Dahbi, *ACS Applied Materials & Interfaces*, 2024, **16**, 2193–2203.

21 F. Zhang, J. You, X. Tang, J. Wang, X. Gong, A. Canizarès, L. Lu and K. Tang, *Journal of Molecular Liquids*, 2023, **387**, 122485.

22 K. Zhang, Y. Duan, N. Graham and W. Yu, *Journal of Hazardous Materials*, 2022, **444**, 130327.

23 C. Yang, C. Pei, R. Luo, S. Liu, Y. Wang, Z. Wang, Z.-J. Zhao and J. Gong, *Journal of the American Chemical Society*, 2020, **142**, 19523–19531.

24 Y. Pu, L. Wang, L. Jia, X. Li, W. Lu and L. Huang, *Applied Surface Science*, 2023, **636**, 157647.

25 M. Chen, Y. Zhang, J. Chen, R. Wang, B. Zhang, B. Song and P. Xu, *Small*, 2024, 2309371.

26 W. Guo, H. Luo, D. Fang, Z. Jiang, J. Chi and W. Shangguan, *Journal of Energy Chemistry*, 2022, **70**, 373–381.

27 R. N. Samajdar, S. Marchesini, S. A. Brown, S. D. Robertson, K. R. Paton, A. J. Pollard and A. J. Wain, *ACS Energy Letters*, 2023, **8**, 1864–1869.

28 J. Zhao, F. Wang, X. Lu, T. Lv, Y. Li, Q. Hao, L. Liang and H. Liu, *Journal of Colloid and Interface Science*, 2023, **642**, 532–539.

29 R. Qin, P. Wang, Z. Li, J. Zhu, F. Cao, H. Xu, Q. Ma, J. Zhang, J. Yu and S. Mu, *Small*, 2021, **18**, 2105305.

30 Y. Zhou, Y. Shen and H. Li, *Applied Catalysis B: Environment and Energy*, 2022, **317**, 121776.

31 Y. Chen, J. Wang, Z. Yu, Y. Hou, R. Jiang, M. Wang, J. Huang, J. Chen, Y. Zhang and H. Zhu, *Applied Catalysis B: Environment and Energy*, 2022, **307**, 121151.

32 S. Li, B. Zhao, A. Aguirre, Y. Wang, R. Li, S. Yang, I. Aravind, Z. Cai, R. Chen, L. Jensen and S. B. Cronin, *Analytical Chemistry*, 2021, **93**, 6421–6427.

33 M. Ziemba, J. Weyel and C. Hess, *Applied Catalysis B: Environment and Energy*, 2021, **301**, 120825.

34 D. Jero, N. Caussé, O. Marsan, T. Buffeteau, F. Chaussec, A. Buvignier, M. Roy and N. Pébère, *Electrochimica Acta*, 2023, **443**, 141925.

35 Y. Xie, L. Sun, X. Pan, Z. Zhou and G. Zhao, *Applied Catalysis B: Environment and Energy*, 2023, **338**, 123068.
36 J. Chen, S. Xiong, H. Liu, J. Shi, J. Mi, H. Liu, Z. Gong, L. Oliviero, F. Maugé and J. Li, *Nature Communications*, 2023, **14**, 3477.
37 Y. Xie, J. Chen, X. Wu, J. Wen, R. Zhao, Z. Li, G. Tian, Q. Zhang, P. Ning and J. Hao, *ACS Catalysis*, 2022, **12**, 10587–10602.
38 X. Yu, H. Tian, Z. Fu, F. Pei, L. Peng, G. Meng, F. Kong, Y. Chen, C. Chen, Z. Chang, X. Cui and J. Shi, *ACS Catalysis*, 2023, **13**, 2834–2846.
39 N. Ferreira, L. Coronel, M. Moreno, L. Cornaglia and J. Múnera, *Fuel Processing Technology*, 2021, **217**, 106814.
40 Y. Wei, Y. Zhang, P. Zhang, J. Xiong, X. Mei, Q. Yu, Z. Zhao and J. Liu, *Environmental Science & Technology*, 2020, **54**, 2002–2011.
41 J. Tang, Q. Ruan, H. Yu and C. Huang, *Advanced Sustainable Systems*, 2023, **7**, 2200473.
42 V. Kamboj, S. Raychowdhury and C. Ranjan, *Applied Catalysis B: Environment and Energy*, 2023, **344**, 123631.
43 Z. Chen, H. Yang, S. Mebs, H. Dau, M. Driess, Z. Wang, Z. Kang and P. W. Menezes, *Advanced Materials*, 2022, **35**, 2208337.
44 L. Zhang, X. Li, L. Chen, C. Zhai and H. Tao, *Journal of Colloid and Interface Science*, 2023, **640**, 783–790.
45 J. Wu, Y. Zhang, B. Zhang, S. Li and P. Xu, *ACS Applied Materials & Interfaces*, 2022, **14**, 14235–14242.
46 Y. Ren, C. Yu, L. Wang, X. Tan, Z. Wang, Q. Wei, Y. Zhang and J. Qiu, *Journal of the American Chemical Society*, 2022, **144**, 10193–10200.
47 H. Sun, L. Chen, Y. Lian, W. Yang, L. Lin, Y. Chen, J. Xu, D. Wang, X. Yang, M. H. Rümmerli, J. Guo, J. Zhong, Z. Deng, Y. Jiao, Y. Peng and S. Qiao, *Advanced Materials*, 2020, **32**, 2006784.
48 Y. Shi, K. Sun, J. Shan, H. Li, J. Gao, Z. Chen, C. Sun, Y. Shuai and Z. Wang, *ACS Catalysis*, 2022, **12**, 8252–8258.
49 M. Guo, B. M. Lis, M. E. Ford and I. E. Wachs, *Applied Catalysis B: Environment and Energy*, 2022, **306**, 121108.
50 S. Jiang, L. D'Amario and H. Dau, *ChemSusChem*, 2022, **15**, e202102506.
51 T. Liang, Z. Dai, Y. Liu, X. Zhang and H. Zeng, *Science Bulletin*, 2021, **66**, 2471–2478.
52 H. Sun, C.-W. Tung, Y. Qiu, W. Zhang, Q. Wang, Z. Li, J. Tang, H.-C. Chen, C. Wang and H. M. Chen, *Journal of the American Chemical Society*, 2021, **144**, 1174–1186.
53 J. Liu, Y. Li, Y. Wang, C. Xiao, M. Liu, X. Zhou, H. Jiang and C. Li, *Nano Research*, 2021, **15**, 1409–1414.
54 S. K. Pahari and Y.-T. Chen, *ACS Applied Materials & Interfaces*, 2022, **14**, 5177–5182.
55 Y. Yang, Z. Tan, J. Zhang, J. Yang, R. Zhang, S. Wang, Y. Song and Z. Su, *Green Energy & Environment*, 2023, **9**, 1459–1465.
56 C. Zhao, C. Wang, H. Xin, H. Li, R. Li, B. Wang, W. Wei, Y. Cui and Q. Fu, *ACS Applied Materials & Interfaces*, 2022, **14**, 26194–26203.
57 X. Liu, Y. Xie, M. Hao, Z. Chen, H. Yang, G. I. Waterhouse, S. Ma and X. Wang, *Advanced Science*, 2022, **9**, 2201735.
58 S. Wen, J. Huang, T. Li, W. Chen, G. Chen, Q. Zhang, X. Zhang, Q. Qian and K. K. Ostrikov, *Applied Catalysis B: Environment and Energy*, 2022, **316**, 121678.
59 K. H. Cho, S. Park, H. Seo, S. Choi, M. Y. Lee, C. Ko and K. T. Nam, *Angewandte Chemie International Edition*, 2021, **60**, 4673–4681.
60 D. Zhang, Y. Li, P. Wang, J. Qu, Y. Li and S. Zhan, *Nature Communications*, 2023, **14**, 3538.
61 H. A. Alzahrani and J. J. Bravo-Suárez, *Journal of Catalysis*, 2023, **418**, 225–236.
62 J.-Z. Zhang, Z. Zhang, H.-B. Zhang, Y. Mei, F. Zhang, P.-X. Hou, C. Liu, H.-M. Cheng and J.-C. Li, *Nano Letters*, 2023, **23**, 8331–8338.
63 W. Chang, J. Qu, W. Li, Y.-H. Liu, X.-Z. Zhai, H.-J. Liu, Y. Kang and Z.-Z. Yu, *Small*, 2021, **17**, 2101857.
64 M. Graf, G. B. Vonbun-Feldbauer and M. T. M. Koper, *ACS Nano*, 2021, **15**, 3188–3200.
65 F. Yang, M. L. Luna, F. T. Haase, D. Escalera-López, A. Yoon, M. Rüscher, C. Rettenmaier, H. S. Jeon, E. Ortega, J. Timoshenko, A. Bergmann, S. W. Chee and B. R. Cuenya, *Journal of the American Chemical Society*, 2023, **145**, 21465–21474.
66 Y. H. Park, S. B. Patil, X. Jin and S.-J. Hwang, *Nano Energy*, 2023, **113**, 108566.
67 H. Li, P. Wei, D. Gao and G. Wang, *Current Opinion in Green and Sustainable Chemistry*, 2022, **34**, 100589.
68 C. Duan, C. Tang, S. Yu, L. Li, J. Li and Y. Zhou, *Applied Catalysis B: Environment and Energy*, 2022, **324**, 122255.
69 P. F. Wu, Y. Q. Yang, H. Y. Xi1, Y. Si, Y. H. Chu, X. Z. Su, W. S. Yan, T. T. You, Y. K. Gao, Y. Wang, W. X. Chen, Y. Y. Huang and P. G. Yin, *Small*, 2023, **20**, 2306716.
70 X. Du, M. Chen, S. Shen, P. Zhou, K. H. Lo and H. Pan, *Materials Today Energy*, 2022, **27**, 101046.
71 J. Hao, H. Zhu, Y. Li, P. Liu, S. Lu, F. Duan, W. Dong, Y. Lu, T. Liu and M. Du, *Chemical Engineering Journal*, 2020, **404**, 126523.
72 Y. Wu, S. Sourav, A. Worrad, J. Zhou, S. Caratzoulas, G. Tsilomelekis, W. Zheng and D. G. Vlachos, *ACS Catalysis*, 2023, **13**, 7371–7382.
73 H. Zhu, Z. Zhu, J. Hao, S. Sun, S. Lu, C. Wang, P. Ma, W. Dong and M. Du, *Chemical Engineering Journal*, 2021, **431**, 133251.
74 Z. Hou, C. Cui, Y. Yang and T. Zhang, *Small*, 2023, **19**, 2207170.
75 H. Xiao, S. Li, J. Zhou, C. Zhao, Y. Yuan, X. Xia, Y. Bao, M. Lourenço, K. Homewood and Y. Gao, *Energy & Environmental Materials*, 2022, **6**, e12537.
76 X. Wang, W. Wang, B. Liu, Z. Song, Z. Ren and H. Fu, *Small*, 2023, **19**, 2304084.
77 E. S. Davydova, M. Manikandan, D. R. Dekel and S. Sunde, *ACS Applied Energy Materials*, 2021, **4**, 3404–3423.
78 M. Tan, T. Li, Y. Zhu, B. Shang and J. Dang, *Journal of Molec-*

ular Liquids, 2021, **331**, 115767.
79 W. Tang, Z. Yu, H. Chen, R. Jiang, J. Huang, S. Li, Y. Hou, M. Wang, H. Pang and J. Liu, *Journal of Colloid and Interface Science*, 2023, **644**, 358–367.
80 Y. Fu, D. Zhang, P. Li, Y. Han, J. You, Q. Wei and W. Yang, *Electrochimica Acta*, 2023, **451**, 142294.
81 F. Xi, F. Bozheyev, X. Han, M. Rusu, J. Rappich, F. F. Abdi, P. Bogdanoff, N. Kaltsoyannis and S. Fiechter, *ACS Applied Materials & Interfaces*, 2022, **14**, 52815–52824.
82 P.-C. Liao, R.-H. Jhang, Y.-H. Chiu, J. A. A. Valinton, C.-H. Yeh, V. D. Ebajo Jr, C.-H. Wang and C.-H. Chen, *ACS Applied Energy Materials*, 2021, **4**, 3448–3459.
83 H. Wang, Y. Song, V. C. Ferrari, N. S. Kim, S. B. Lee, P. Albertus, G. Rubloff and D. M. Stewart, *ACS Applied Materials & Interfaces*, 2023, **15**, 40409–40418.
84 Q. Li, Q. Chen, K. Jiang, S. Lei, Y. Deng and J. Bao, *International Journal of Hydrogen Energy*, 2023, **48**, 17501–17511.
85 K. Xu, Z. Wang, C. He, S. Ruan, F. Liu and L. Zhang, *ACS Applied Energy Materials*, 2021, **4**, 13226–13238.
86 Y. Zhu, X. Wang, X. Zhu, Z. Wu, D. Zhao, F. Wang, D. Sun, Y. Tang, H. Li and G. Fu, *Small*, 2022, **19**, 2206531.
87 D. Li, Y. Qin, J. Liu, H. Zhao, Z. Sun, G. Chen, D.-Y. Wu, Y. Su, S. Ding and C. Xiao, *Advanced Functional Materials*, 2021, **32**, 2107056.
88 C. Huang, B. Zhang, Y. Wu, Q. Ruan, L. Liu, J. Su, Y. Tang, R. Liu and P. K. Chu, *Applied Catalysis B: Environment and Energy*, 2021, **297**, 120461.
89 X. Ding, R. Jiang, J. Wu, M. Xing, Z. Qiao, X. Zeng, S. Wang and D. Cao, *Advanced Functional Materials*, 2023, **33**, 2306786.
90 F. Braga, G. Casano, L. M. Daniels, M. Caffio and L. J. Hardwick, *Electrochimica Acta*, 2023, **455**, 142433.
91 C. Fan, X. Wang, X. Wu, Y. Chen, Z. Wang, M. Li, D. Sun, Y. Tang and G. Fu, *Advanced Energy Materials*, 2023, **13**, 2203244.
92 X. Zhang, C. Feng, B. Dong, C. Liu and Y. Chai, *Advanced Materials*, 2023, **35**, 2207066.
93 W. He, R. Zhang, H. Liu, Q. Hao, Y. Li, X. Zheng, C. Liu, J. Zhang and H. L. Xin, *Small*, 2023, **19**, 2301610.
94 M. Pei, T. Li, G. Chen and K. K. Ostrikov, *International Journal of Hydrogen Energy*, 2023, **51**, 975–987.
95 J. Zhang, R. Djellabi, S. Zhao, M. Qiao, F. Jiang, M. Yan and X. Zhao, *Journal of Hazardous Materials*, 2020, **394**, 122559.
96 C. Lee, Y. Yokoyama, Y. Kondo, Y. Miyahara, T. Abe and K. Miyazaki, *ACS Applied Materials & Interfaces*, 2020, **12**, 56076–56085.
97 B. Han, Y. Gao, L. Zhu, Z. Ma, X. Zhang, H. Ding and Y. Zhang, *Advanced Materials Technologies*, 2020, **5**, 1900963.
98 C. Liu, G. Zhang, W. Zhou, K. Zhang, J. Qu and H. Liu, *ACS Applied Materials & Interfaces*, 2021, **13**, 18673–18682.
99 Z. Tu, X. Liu, D. Xiong, J. Wang, S. Gong, C. Xu, D. Wu and Z. Chen, *Chemical Engineering Journal*, 2023, **475**, 146253.
100 J. Choi, D. Kim, W. Zheng, B. Yan, Y. Li, L. Y. S. Lee and Y. Piao, *Applied Catalysis B: Environment and Energy*, 2021, **286**, 119857.
101 Y. Wu, Z. Xie, Y. Li, Z. Lv, L. Xu and B. Wei, *International Journal of Hydrogen Energy*, 2021, **46**, 25070–25080.
102 J. Hu, A. Al-Salihy, J. Wang, X. Li, Y. Fu, Z. Li, X. Han, B. Song and P. Xu, *Advanced Science*, 2021, **8**, 2103314.
103 Y. Wei, L. Yi, R. Wang, J. Li, D. Li, T. Li, W. Sun and W. Hu, *Small*, 2023, **19**, 2301267.
104 L. Li, L. Zhang, L. Gou, S. Wei, X. Hou and L. Wu, *Chemical Engineering Journal*, 2023, **454**, 140292.
105 J. N. Hausmann, P. V. Menezes, G. Vijaykumar, K. Laun, T. Diemant, I. Zebger, T. Jacob, M. Driess and P. W. Menezes, *Advanced Energy Materials*, 2022, **12**, 2202098.
106 D. Kiani, S. Sourav, J. Baltrusaitis and I. E. Wachs, *ACS Catalysis*, 2021, **11**, 10131–10137.
107 Y. Zhang, J. Yang, Z. Yu, Y. Hou, R. Jiang, J. Huang, F. Yang, S. Yao, L. Gao and W. Tang, *Chemical Engineering Journal*, 2021, **416**, 129124.
108 Q.-N. Wang, X. Sun, Z. Feng, Z. Feng, P. Zhang, Y. Zhang and C. Li, *ACS Catalysis*, 2022, **12**, 3323–3332.
109 H. Yin, H. Xiao, R. Qin, J. Chen, F. Tan, W. Zhang, J. Zhao, L. Zeng, Y. Hu, F. Pan, P. Lei, S. Yuan, L. Qian, Y. Su and Z. Zhang, *ACS Applied Materials & Interfaces*, 2023, **15**, 20100–20109.
110 X. Liu, W. Chen, C. Zhang, T. Li, J. Huang, G. Chen, T. Shao, T. Gong and K. Ostrikov, *ACS Sustainable Chemistry & Engineering*, 2022, **10**, 8064–8074.
111 Z. Wen, F. Wu, L. Li, N. Chen, G. Luo, J. Du, L. Zhao, Y. Ma, Y. Li and R. Chen, *ACS Applied Materials & Interfaces*, 2022, **14**, 38807–38814.
112 K. Wang, H. Yang, Q. Wang, J. Yu, Y. He, Y. Wang, S. Song and Y. Wang, *Advanced Energy Materials*, 2023, **13**, 2204371.
113 C. Wei, Y. Yang, H. Ma, G. Sun, X. Wang, Y. Cheng, C. Zhang, B. S. Yeo, C. He and A. B. Wong, *Advanced Functional Materials*, 2023, **33**, 2214992.
114 P. W. Menezes, S. Yao, R. Beltrán-Suito, J. N. Hausmann, P. V. Menezes and M. Driess, *Angewandte Chemie*, 2021, **133**, 4690–4697.
115 X. Peng, C. Huang, J. Dai and Y. Liu, *International Journal of Hydrogen Energy*, 2021, **47**, 4386–4393.
116 J. Yu, M. Yang, Z. Li, C. Liu, Y. Wei, C. Zhang, B. Man and F. Lei, *Analytical Chemistry*, 2020, **92**, 14754–14761.
117 Y. Sun, G. Xu, Y. Wang, W. Shi, Y. Yu and H. He, *Environmental Science & Technology*, 2023, **57**, 20370–20379.
118 J.-J. Liu, Z.-W. Jiang and S.-W. Hsu, *ACS Applied Materials & Interfaces*, 2023, **15**, 6716–6725.
119 D. M. Josepetti, B. P. Sousa, S. A. J. Rodrigues, R. G. Freitas and G. Doubek, *Journal of Energy Chemistry*, 2023, **88**, 223–231.
120 G. J. Myres and J. M. Harris, *Analytical Chemistry*, 2023, **95**, 3499–3506.
121 S. Y. Chun, S. Park, S. I. Lee, H. D. Nguyen, K.-K. Lee, S. Hong, C.-H. Han, M. Cho, H.-K. Choi and K. Kwak, *Nano*

Energy, 2021, **82**, 105721.
122 B. Liu, R. Feng, M. Busch, S. Wang, H. Wu, P. Liu, J. Gu, A. Bahadoran, D. Matsumura, T. Tsuji, D. Zhang, F. Song and Q. Liu, *ACS Nano*, 2022, **16**, 14121–14133.
123 M. Nadjafi, P. M. Abdala, R. Verel, D. Hosseini, O. V. Safonova, A. Fedorov and C. R. Müller, *ACS Catalysis*, 2020, **10**, 2314–2321.
124 F. Lyu, B. Ma, X. Xie, D. Song, Y. Lian, H. Yang, W. Hua, H. Sun, J. Zhong, Z. Deng, T. Cheng and Y. Peng, *Advanced Functional Materials*, 2023, **33**, 2214609.
125 Q. Zeng, Y. Wen, X. Duan, X. Xu, J. Tan, Q. Zhang, Y. Liu and Q. Zeng, *Applied Catalysis B: Environment and Energy*, 2024, **346**, 123752.
126 M. Guo, B. M. Lis, M. E. Ford and I. E. Wachs, *Applied Catalysis B: Environment and Energy*, 2022, **306**, 121128.
127 Y. Xu, J. Wang, S. Wang, Z. Zhai, B. Ren, Z. Tian, L. Zhang and Z. Liu, *International Journal of Hydrogen Energy*, 2023, **48**, 34340–34354.
128 M. Li, Y. Hu, W. Fang, S. Xin, Y. Wu, Y. Cao, W. Cui, Z. Li and H. Zhao, *Chemical Engineering Journal*, 2023, **480**, 148014.
129 G. Li, Y. Song, C. Zhu, X. Dong, W. Chen, G. Wu, G. Feng, S. Li and W. Wei, *Journal of CO2 Utilization*, 2023, **70**, 102446.
130 Q. Huang, Z. Xi and W. Wei, *Journal of Alloys and Compounds*, 2020, **843**, 155971.
131 S. Sourav, Y. Wang, D. Kiani, J. Baltrusaitis, R. R. Fushimi and I. E. Wachs, *Angewandte Chemie International Edition*, 2021, **60**, 21502–21511.
132 J. Liu, J. Jiang, M. Wang, J. Kang, J. Zhang, S. Liu, Y. Tang and S. Li, *Separation and Purification Technology*, 2022, **294**, 121082.
133 Y. Yang, Y. Li, W. Zhai, X. Li, D. Li, H. Lin and S. Han, *Analytical Chemistry*, 2020, **93**, 946–955.
134 C. Liu, F. Lei, M. Gong, X. Zhou, X. Zhao, Z. Li, C. Zhang, B. Man and J. Yu, *Energy & Environmental Materials*, 2022, **7**, e12517.
135 J. Dou, Y. Tang, Z. Lu, G. He, J. Xu and Y. He, *Environmental Science & Technology*, 2023, **57**, 5703–5713.
136 J. Yang, P. Li, X. Duan, D. Zeng, Z. Ma, S. An, L. Dong, W. Cen and Y. He, *Journal of Hazardous Materials*, 2022, **430**, 128463.
137 W. Qu, Z. Tang, S. Tang, H. Wen, J. Fang, Q. Lian, D. Shu and C. He, *Advanced Functional Materials*, 2023, **33**, 2301677.
138 D. Kiani, S. Sourav, W. Taifan, M. Calatayud, F. Tielens, I. E. Wachs and J. Baltrusaitis, *ACS Catalysis*, 2020, **10**, 4580–4592.
139 K. Dang, H. Dong, L. Wang, M. Jiang, S. Jiang, W. Sun, D. Wang and Y. Tian, *Advanced Materials*, 2022, **34**, 2200302.
140 N. A. Gvozdik and K. J. Stevenson, *Electrochimica Acta*, 2021, **383**, 138300.
141 J. Chen, G. Liu, Y.-z. Zhu, M. Su, P. Yin, X.-j. Wu, Q. Lu, C. Tan, M. Zhao, Z. Liu, W. Yang, H. Li, G.-H. Nam, L. Zhang, Z. Chen, X. Huang, P. M. Radjenovic, W. Huang, Z.-q. Tian, J.-f. Li and H. Zhang, *Journal of the American Chemical Society*, 2020, **142**, 7161–7167.
142 W. G. Nunes, B. M. Pires, F. E. D. Oliveira, A. M. de Marque, L. F. Cremasco, R. Vicentini, G. Doubek, L. M. D. Silva and H. Zanin, *Journal of Energy Storage*, 2020, **28**, 101249.
143 Y. Yu, D. Wei, Z. Tong, J. Wang, J. Chen and C. He, *Chemical Engineering Journal*, 2022, **442**, 136356.
144 T. Li, C. Tang, H. Guo, H. Wu, C. Duan, H. Wang, F. Zhang, Y. Cao, G. Yang and Y. Zhou, *ACS Applied Materials & Interfaces*, 2022, **14**, 49765–49773.
145 Y. Wen, Z. Zhuang, H. Zhu, J. Hao, K. Chu, F. Lai, W. Zong, C. Wang, P. Ma, W. Dong, S. Lu, T. Liu and M. Du, *Advanced Energy Materials*, 2021, **11**, 2102138.
146 A. Nekrasov, O. Iakobson and O. Gribkova, *Electrochimica Acta*, 2021, **390**, 138869.
147 Y. Chen, Y. Zhu, H. Sheng, J. Wang, C. Zhang, Y. Chen, W. Huang and G. Lu, *ACS Catalysis*, 2022, **12**, 2938–2946.
148 L. Fu, Z. Qu, L. Zhou and Y. Ding, *Applied Catalysis B: Environment and Energy*, 2023, **339**, 123170.
149 Y. Tao, S. Fan, X. Li, J. Yang, J. Wang and G. Chen, *Journal of Colloid and Interface Science*, 2024, **654**, 731–739.
150 R. Hao, S. Fang, L. Tian, R. Xia, Q. Guan, L. Jiao, Y. Liu and W. Li, *Chemical Engineering Journal*, 2023, **467**, 143371.
151 S. Dai, W. Zhang, T. Xia, H. Hu, Z. Zhang and X. Li, *Scripta Materialia*, 2022, **215**, 114691.
152 D. Kotlarek, S. Fossati, P. Venugopalan, N. G. Quilis, J. Slabý, J. Homola, M. Lequeux, F. Amiard, M. L. de la Chapelle, U. Jonas and J. Dostálek, *Nanoscale*, 2020, **12**, 9756–9768.
153 C. Li, S. Li, A. Qu, H. Kuang, L. Xu and C. Xu, *Advanced Functional Materials*, 2020, **30**, 2001451.
154 Z. Li, C. Zhang, H. Sheng, J. Wang, Y. Zhu, L. Yu, J. Wang, Q. Peng and G. Lu, *ACS Applied Materials & Interfaces*, 2022, **14**, 38302–38310.
155 K. K. Rani, Q. Yang, Y.-H. Xiao, R. Devasenathipathy, Z. Lu, X. Chen, L. Jiang, Z. Li, Q. Liu, H. Chen, L. Yu, Z. Li, S. Khayour, J. Wang, K. Wang, G. Li, D.-Y. Wu and G. Lu, *ACS Applied Materials & Interfaces*, 2023, **15**, 57818–57827.
156 L. Tian, R. Hao, Y.-X. Zhou, Y. Zhang, Q.-X. Guan, Y.-P. Liu and W. Li, *ACS Sustainable Chemistry & Engineering*, 2023, **11**, 15865–15875.
157 H. Yu, Y. Long, D. Chen, X. Dong, X. Ye, Y. Zhang, F. Li, Y. Xu, Y. Tao and Q.-H. Yang, *Small*, 2023, **20**, 2303832.
158 P. Shao, Y. Liao, X. Feng, C. Yan, L. Ye and J. Yang, *Journal of Colloid and Interface Science*, 2023, **633**, 199–206.
159 P. P. Paalanen, S. H. van Vreeswijk and B. M. Weckhuysen, *ACS Catalysis*, 2020, **10**, 9837–9855.
160 X. Zheng, X. Yan, J. Ma, X. Yao, J. Zhang and L. Wang, *ACS Applied Materials & Interfaces*, 2021, **13**, 16498–16506.
161 B. Long, J. Ma, T. Song, X. Wang and Y. Tong, *Electrochimica Acta*, 2021, **374**, 137934.
162 A. Kong, M. Liu, H. Zhang, Z. Cao, J. Zhang, W. Li, Y. Han and Y. Fu, *Chemical Engineering Journal*, 2022, **445**, 136719.
163 S. Li, T. Wang, D. Tang, Y. Yang, Y. Tian, F. Cui, J. Sun, X. Jing, D. S. Sholl and G. Zhu, *Advanced Science*, 2022, **9**,

2203712.

164 J. Li, G. Wang, L. Yu, J. Gao, Y. Li, S. Zeng and G. Zhang, *ACS Applied Materials & Interfaces*, 2021, **13**, 13139–13148.

165 A. A. Papaderakis, A. Ejigu, J. Yang, A. Elgendy, B. Radha, A. Keerthi, A. Juel and R. A. W. Dryfe, *Journal of the American Chemical Society*, 2023, **145**, 8007–8020.

166 W. Yang, M. Li, B. Zhang, Y. Liu, J. Zi, H. Xiao, X. Liu, J. Lin, H. Zhang, J. Chen, Z. Wan, Z. Li, G. Li, H. Li and Z. Lian, *Advanced Functional Materials*, 2023, **33**, 2304852.

167 L. Han, Y. Zhou, Z. Tan, H. Zhu, Y. Hu, X. Ma, F. Zheng, F. Feng, C. Wang and W. Liu, *Analytical Chemistry*, 2023, **95**, 6312–6322.

168 H. Yan, S. Alayoglu, W. Wu, Y. Zhang, E. Weitz, P. C. Stair and J. M. Notestein, *ACS Catalysis*, 2021, **11**, 9370–9376.

169 X. You, D. Zhang, X.-G. Zhang, X. Li, J.-H. Tian, Y.-H. Wang and J.-F. Li, *Nano-Micro Letters*, 2024, **16**, 53.

170 Y. Li, C. Li, R. Li, X. Peng, J. Zhang, P. Yang, G. Wang, B. Wang, P. Broekmann and M. An, *ACS applied materials & interfaces*, 2023, **15**, 47628–47639.

171 Z. Wang, J. Liu, X. Wu, N. Nie, D. Zhang, H. Li, H. Zhao, J. Lai and L. Wang, *Applied Catalysis B: Environment and Energy*, 2022, **314**, 121465.

172 M. P. L. Kang, H. Ma, R. Ganganahalli and B. S. Yeo, *ACS Catalysis*, 2023, **14**, 116–123.

173 H. Zhang, Y. Sun, J. Wang, X. Gao, Z. Tang, S. Li, Z. Hou, X. Wang, K. Nie, J. Xie, Z. Yang and Y.-M. Yan, *ACS Applied Energy Materials*, 2023, **6**, 11448–11457.

174 S. Mu, L. Li, R. Zhao, H. Lu, H. Dong and C. Cui, *ACS Applied Materials & Interfaces*, 2021, **13**, 47619–47628.

175 D. Xiong, X. He, X. Liu, S. Gong, C. Xu, Z. Tu, D. Wu, J. Wang and Z. Chen, *Small*, 2023, **20**, 2306100.

176 J. Gao, Y. Meng, A. Benton, J. He, L. G. Jacobsohn, J. Tong and K. S. Brinkman, *ACS applied materials & interfaces*, 2020, **12**, 38012–38018.

177 Z. Zhu, L. Luo, Y. He, M. Mushtaq, J. Li, H. Yang, Z. Khanam, J. Qu, Z. Wang and M.-S. Balogun, *Advanced Functional Materials*, 2023, **34**, 2306061.

178 M. N. Polyanskiy, *Scientific Data*, 2024, **11**, 94.

179 W. S. Werner, K. Glantschnig and C. Ambrosch-Draxl, *Journal of Physical and Chemical Reference Data*, 2009, **38**, 1013–1092.

180 V. Nemoshkalenko, V. Antonov, M. Kirillova, A. Krasovskii, L. Nomerovannaya *et al.*, *Zh. Eksp. Teor. Fiz.*, 1986, **90**, 201–208.

181 P. Schmitt, N. Felde, T. Döhring, M. Stollenwerk, I. Uschmann, K. Hanemann, M. Siegler, G. Klemm, N. Gratzke, A. Tünnermann *et al.*, *Optical Materials Express*, 2022, **12**, 545–559.